AD-A204 682

Technical Document 1307
December 1988

The Effect of the Conventional Beampattern on Adaptive Beamformer Performance

S. K. Lapic
J. C. Lockwood
D. F. Gingras

DTIC
ELECTE
FEB 2 2 1989
S D
H

89 2 17 016

Approved for public release; distribution is unlimited.

REPORT DOCUMENTATION PAGE

1a. REPORT SECURITY CLASSIFICATION UNCLASSIFIED	1b. RESTRICTIVE MARKINGS
2a. SECURITY CLASSIFICATION AUTHORITY	3. DISTRIBUTION/AVAILABILITY OF REPORT
2b. DECLASSIFICATION/DOWNGRADING SCHEDULE	Approved for public release; distribution is unlimited.
4. PERFORMING ORGANIZATION REPORT NUMBER(S) NOSC TD 1307	5. MONITORING ORGANIZATION REPORT NUMBER(S)
6a. NAME OF PERFORMING ORGANIZATION Naval Ocean Systems Center 6b. OFFICE SYMBOL (if applicable) Code 733	7a. NAME OF MONITORING ORGANIZATION
6c. ADDRESS (City, State and ZIP Code) San Diego, CA 92152-5000	7b. ADDRESS (City, State and ZIP Code)
8a. NAME OF FUNDING/SPONSORING ORGANIZATION Office of Chief of Naval Research 8b. OFFICE SYMBOL (if applicable)	9. PROCUREMENT INSTRUMENT IDENTIFICATION NUMBER
8c. ADDRESS (City, State and ZIP Code) Arlington, VA 22217-5000	10. SOURCE OF FUNDING NUMBERS PROGRAM ELEMENT NO.: 61152N PROJECT NO.: ZT76 TASK NO.: AGENCY ACCESSION NO.: DN307 410

11. TITLE (include Security Classification)

THE EFFECT OF THE CONVENTIONAL BEAMPATTERN ON ADAPTIVE BEAMFORMER PERFORMANCE

12. PERSONAL AUTHOR(S)

S. K. Lapic, J. C. Lockwood, D. F. Gingras

13a. TYPE OF REPORT	13b. TIME COVERED	14. DATE OF REPORT (Year, Month, Day)	15. PAGE COUNT
Final	FROM TO	December 1988	62

16. SUPPLEMENTARY NOTATION

17. COSATI CODES			18. SUBJECT TERMS (Continue on reverse if necessary and identify by block number)
FIELD	GROUP	SUB-GROUP	spurious peaks, adaptive array, array response, random arrays,

19. ABSTRACT (Continue on reverse if necessary and identify by block number)

This report develops an expression that relates the adaptive beamformer array response function to the conventional beamformer beampattern function in the sidelobe region. Specific examples for deterministic, randomized, and random arrays are evaluated. These examples clearly indicate that sidelobes in the conventional beampattern function produce spurious peaks in the adaptive array response. The probability that a spurious peak exceeds a threshold for the adaptive array response of random arrays is developed. The probability that a signal peak exceeds the peak spurious peak for minimum-energy adaptive beamforming with random arrays is developed.

20. DISTRIBUTION/AVAILABILITY OF ABSTRACT	21. ABSTRACT SECURITY CLASSIFICATION
☐ UNCLASSIFIED/UNLIMITED ☒ SAME AS RPT ☐ DTIC USERS	UNCLASSIFIED

22a. NAME OF RESPONSIBLE PERSON	22b. TELEPHONE (include Area Code)	22c. OFFICE SYMBOL
J. C. Lockwood	(619) 553-2057	Code 733

DD FORM 1473, 84 JAN

83 APR EDITION MAY BE USED UNTIL EXHAUSTED
ALL OTHER EDITIONS ARE OBSOLETE

CONTENTS

DTIC COPY INSPECTED 6

Accession For
NTIS GRA&I ☑
DTIC TAB ☐
Unannounced ☐
Justification
By
Distribution/
Availability Codes
Dist | Avail and/or Special
A-1

I. INTRODUCTION

One measure of the "goodness" of an antenna or sensor array is the sidelobe structure of the beampattern function when the conventional linear beamformer is used. In this report, we examine the performance of the adaptive beamformer in terms of spurious peaks in the array response function by exploiting the relation between adaptive array response and the conventional beampattern. An expression that provides an approximate relationship between the array response function for an adaptive beamformer and the conventional beampattern function in the sidelobe region is developed. The validity of the approximation is examined using simulations for a variety of arrays including deterministic, randomized, and random cases. The approximate relationship is used to obtain the probability that a spurious peak in the adaptive array response exceeds a threshold for random arrays.

The organization of the report is as follows: In Sections II and III, the basic relationships for conventional and adaptive beamforming are established. In Section IV, the approximate relationship between adaptive array response and conventional beampatterns is developed. In Sections V and VI, the relationship is validated through simulation. In Section VII, the spurious peak estimator for random arrays is developed.

II. CONVENTIONAL BEAMFORMING AND BEAMPATTERNS

The relationship between the beampatterns or power patterns of an array and the observed array response patterns when using conventional beamforming is fairly straightforward. For example, when the noise field consists of a single signal from a (multidimensional) arrival angle θ, the conventional array-response pattern (normalized to 0 dB at θ) would simply be the conventional beampattern steered at the signal

$$|\mathbf{S}_{\theta}^{*}\mathbf{S}_{\text{look}}|^2 \ . \tag{1}$$

Here, the vector $\mathbf{S}$ represents an ideal plane wave and has the form

$$\mathbf{S} = \frac{1}{\sqrt{N}} \begin{bmatrix} \exp\ i\frac{\omega}{c} < z_1,\ \kappa > \\ \vdots \\ \exp\ i\frac{\omega}{c} < z_N,\ \kappa > \end{bmatrix} . \tag{2}$$

The convention in this report will be to use unit norm signal vectors. Frequently, norm-N vectors are used. When necessary, a factor of N will be explicitly included. The unit vector κ indicates the direction of look or steering angle as well as the direction of arrival of the signal. Element position vectors for the N elements of the array are $\mathbf{z}_1$ through $\mathbf{z}_N$. The inner product is represented by $<\cdot,\cdot>$. Vectors and matrices are denoted by bold-face characters and * denotes complex-conjugate transpose.

More generally, we assume that the time-series data at the array can be written as a vector $\mathbf{X}(t) = \begin{bmatrix} X_1(t) \\ \vdots \\ X_N(t) \end{bmatrix}$. Let $\mathbf{X}(\omega)$ represent a Fourier transform vector

$$\mathbf{X}(\omega) = \frac{1}{T} \int_0^T \mathbf{X}(t)e^{-i\omega t}\ dt \ , \tag{3}$$

where the frequency ω is an integral multiple of $2\pi/T$. The data at frequency ω are then completely described by a cross-spectral matrix $\mathbf{R}$ which is formed by summing outer products of Fourier transform vectors

$$\mathbf{R}(\omega) = \frac{1}{L} \sum_{\ell=1}^{L} \mathbf{X}_{\ell}(\omega)\mathbf{x}_{\ell}^{*}(\omega) \ . \tag{4}$$

If the signal plus noise field consists of K uncorrelated signals S_i of power $\sigma_{s_i}^2$ (i = 1,2,...,K) in noise of power σ_n^2 which is uncorrelated from sensor to sensor, then

$$\mathbf{R} = \sum_{i=1}^{K} N\sigma_{s_i}^2 \mathbf{S}_i\mathbf{S}_i^* + \sigma_n^2\mathbf{I} \ . \tag{5}$$

Another way to write this is

$$\mathbf{R} = \mathbf{ADA}^* + \sigma_n^2\mathbf{I} \ , \tag{6}$$

where $\mathbf{A}$ is the $N \times K$ matrix of discrete signals

$$\mathbf{A} = \left[\mathbf{S}_1 \ \mathbf{S}_2 \ \ldots \ \mathbf{S}_K\right] ,$$

and $\mathbf{D}$ is the diagonal matrix of signal powers

$$\mathbf{D} = \begin{bmatrix} N\sigma_1^2 & & & 0 \\ & N\sigma_2^2 & & \\ & & \ddots & \\ 0 & & & N\sigma_K^2 \end{bmatrix} .$$

The conventional beamformer calculates $\mathbf{S}_{look}^*\mathbf{RS}_{look}$ and peaks in the resulting array-response pattern are identified as signal arrivals. The power output of the conventional beamformer with the signal plus noise field of (6) is

$$\begin{aligned} P_{CBF} &= \mathbf{S}_{look}^*\mathbf{RS}_{look} \\ &= \mathbf{S}_{look}^*\mathbf{ADA}^*\mathbf{S}_{look} + \sigma_n^2 \\ &= \sigma_n^2\left[1 + \sum_{i=1}^{K} \beta_i|\mathbf{S}_i^*\mathbf{S}_{look}|^2\right] \end{aligned} \tag{7}$$

with $\beta_i = N\sigma_{s_i}^2/\sigma_n^2$. The resulting conventional array-response pattern is, thus, heavily dependent on the conventional beampatterns steered at the signals. Figure 1 is the 17-element array. Figure 2 is the conventional beampattern for the 17-element array of figure 1 where it is steered to $\theta = 180°$ in uncorrelated noise. Figure 3 is the conventional array response which results when a single 0-dB signal-to-noise ration (SNR) signal is present in uncorrelated noise. Note that the array-response plot is a scaled version of the beampattern. The sidelobes in the beampattern become spurious peaks in the array-response plot.

III. ADAPTIVE BEAMFORMING

Adaptive beamformers rely on information about the noise field to improve signal detection performance and are capable of extremely high resolution, low bias, and interference rejection. In some cases, adaptive beamformers lack the robustness of conventional beamformers. Nevertheless, the strengths of adaptive techniques are considerable, and they offer a powerful tool for target detection and localization.

One outstanding issue is the impact of an array's conventional beampatterns on its adaptive array response. One might argue, on purely heuristic grounds, that an array that performs poorly using conventional techniques will also have relatively poor adaptive performance. In fact, this is the case. However, we wish to make this relationship more quantitative and relate it to signal detection.

We consider two adaptive beamformers. The first is the minimum-energy (Capon's) beamformer. This is closely allied with the maximum-entropy beamformer described by Burg. The second is the music or eigenvector beamformer which is currently a topic of much interest.

Given a noise field described by a cross-spectral matrix $\mathbf{R}$, the minimum energy beamformer selects a filter vector $\mathbf{W}_{look}$ which minimizes the output power $\mathbf{W}^*_{look}\mathbf{R}\mathbf{W}_{look}$ subject to the constraint that $\mathbf{W}^*_{look}\mathbf{S}_{look} = 1$ where $\mathbf{S}_{look}$ is an ideal plane wave in the look direction. The solution to this constrained optimization problem is found by the method of Lagrange multipliers. We write

$$F = \mathbf{W}^*\mathbf{R}\mathbf{W} + \lambda(\mathbf{W}^*\mathbf{S} - 1) ,$$

and set

$$\frac{\partial F}{\partial \mathbf{W}} = 0 , \frac{\partial F}{\partial \mathbf{W}^*} = 0 , \text{ and } \frac{\partial F}{\partial \lambda} = 0 .$$

The familiar minimum energy steering vector is thus

$$\mathbf{W} = \frac{\mathbf{R}^{-1}\mathbf{S}}{\mathbf{S}^*\mathbf{R}^{-1}\mathbf{S}} , \tag{8}$$

and the output power of the minimum energy beamformer is

$$P_{ME} = \mathbf{W}^*\mathbf{R}\mathbf{W} = \left(\frac{\mathbf{R}^{-1}\mathbf{S}}{\mathbf{S}^*\mathbf{R}^{-1}\mathbf{S}}\right)^* \cdot \mathbf{R} \cdot \left(\frac{\mathbf{R}^{-1}\mathbf{S}}{\mathbf{S}^*\mathbf{R}^{-1}\mathbf{S}}\right) = \frac{1}{\mathbf{S}^*_{look}\mathbf{R}^{-1}\mathbf{S}_{look}} . \tag{9}$$

Return to the noise model of (6), $\mathbf{R} = \mathbf{A}\mathbf{D}\mathbf{A}^* + \sigma_n^2\mathbf{I}$, and assume that the number of signals K is less than the number of array elements N. We note that, provided some basic array design criteria is met, both $\mathbf{A}$ and $\mathbf{A}\mathbf{D}\mathbf{A}^*$ are rank K matrices. Also, since $\mathbf{D}$ is positive-definite, $\mathbf{A}\mathbf{D}\mathbf{A}^*$ is positive semi-definite. We can then write $\mathbf{A}\mathbf{D}\mathbf{A}^*$ in terms of its eigenvalues and eigenvectors as

$$\mathbf{ADA}^* = \sum_{i=1}^{K} \lambda_i \mathbf{V}_i \mathbf{V}_i^* \tag{10}$$

where the eigenvalues λ_i are all strictly positive. The space spanned by the K eigenvectors of $\mathbf{ADA}^*$ associated with positive eigenvalues is also the space spanned by the columns of $\mathbf{ADA}^*$ — the signal vectors. This space is called the signal subspace.

With the result of (10) and the fact that

$$\mathbf{I} = \sum_{i=1}^{N} \mathbf{V}_i \mathbf{V}_i^*$$

for any set of orthonormal vectors $\{\mathbf{V}_i\}$ of length N, we can write

$$\mathbf{R} = \sum_{i=1}^{K} (\lambda_i + \sigma_n^2) \mathbf{V}_i \mathbf{V}_i^* + \sum_{i=K+1}^{N} \sigma_n^2 \mathbf{V}_i \mathbf{V}_i^* . \tag{11}$$

Thus, the K largest eigenvectors (those associated with the K largest eigenvalues) form a basis for the space spanned by the K signal vectors. The (N-K) smallest eigenvectors are orthogonal to the signal subspace and form a basis for the noise-only or noise subspace. Furthermore, the (N-K) smallest eigenvalues are all equal to the noise power σ_n^2.

The second of the two adaptive beamforms we consider, the music beamformer (Johnson, September 1982, and Schmidt, 1979) takes advantage of the orthogonality of the noise-only eigenvectors with the signal vectors. The output of the music beamformer has the form

$$P_{MUSIC} = \frac{1}{\mathbf{S}_{look}^* \left(\sum_{i=K+1}^{N} \frac{1}{\lambda_i} \mathbf{V}_i \mathbf{V}_i^* \right) \mathbf{S}_{look}} . \tag{12}$$

Peaks in the MUSIC response plot corresponding to signal directions of arrival occur when $\mathbf{S}_{look}^*$ is in the signal subspace and the denominator of (12) is zero. Equation (12) is Johnson's (August, 1982) implementation of this beamformer.

Before investigating the array response of these adaptive beamformers, we look at the adaptive beampatterns. An *adaptive* beampattern results when a filter vector $\mathbf{W}_{steer}$ such as the vector of (8) is fixed and $|\mathbf{W}_{steer}^* \mathbf{S}|^2$ is plotted as we sweep an ideal plane-wave S through all directions of arrival. The beampattern is a visual picture of the relative sensitivity of the array to various arrival directions while steered with $\mathbf{W}_{steer}$.

For the conventional beamformer, the beampattern $|\mathbf{S}_{steer}^* \mathbf{S}|^2$ is independent of the noise field. Since the selection of the adaptive steering vector depends on the noise field, however, this is not the case for the adaptive beamformer. The beampattern will be heavily

dependent on the noise field. Figure 4 is the beampattern of the minimum-energy (ME) beamformer of the array of figure 1 steered to $\theta = 180°$ when a 0-dB SNR signal is present at $\theta = 30°$ in uncorrelated noise.

At least one property of adaptive beampatterns can be explored, however. Return to expression (8) for the minimum-energy steering vector. If we write the spectral decomposition of $\mathbf{R}$ as

$$\mathbf{R} = \sum_{i=1}^{N} \lambda_i \mathbf{V}_i \mathbf{V}_i^* ,$$

with $\lambda_1 \geq \lambda \geq \ldots \geq \lambda_N$ and recall that

$$\mathbf{R}^{-1} = \sum_{i=1}^{N} \frac{1}{\lambda_i} \mathbf{V}_i \mathbf{V}_i^* ,$$

then the beampattern becomes:

$$|\mathbf{W}_{steer}^* \mathbf{S}|^2 = \mu^2 |(\mathbf{R}^{-1}\mathbf{S}_{steer})^* \mathbf{S}|^2 \text{ with } \mu = \frac{1}{\mathbf{S}_{steer}^* \mathbf{R}^{-1} \mathbf{S}_{steer}}$$

$$= \mu^2 \left| \left(\left(\sum_{i=1}^{N} \frac{1}{\lambda_i} \mathbf{V}_i \mathbf{V}_i^* \right) \mathbf{S}_{steer} \right)^* \mathbf{S} \right|^2$$

$$= \mu^2 \left| \sum_{i=1}^{N} \frac{\alpha_i^*}{\lambda_i} \mathbf{V}_i^* \mathbf{S} \right|^2 \text{ with } \alpha_i = \mathbf{V}_i^* \mathbf{S}_{steer}$$

Note that for the case of K signals, $\lambda_i >> \sigma_n^2$ i=1,2,...,K. Thus, the contribution to the beampattern due to the signal subspace eigenvectors is much less than that due to the noise subspace. We can then write that

$$|\mathbf{W}_{steer}^* \mathbf{S}|^2 \simeq \mu^2 \left| \sum_{i=K+1}^{N} \frac{\alpha_i^*}{\lambda_i} \mathbf{V}_i^* \mathbf{S} \right|^2 .$$

If we look in the direction of one of the signals (i.e., let $\mathbf{S} = \mathbf{S}_{signal}$), then the adaptive beampattern will have a value

$$|\mathbf{W}_{steer}^* \mathbf{S}_{signal}|^2 \simeq \mu^2 \left| \sum_{i=K+1}^{N} \frac{\alpha_i^*}{\lambda_i} \mathbf{V}_i^* \mathbf{S}_{signal} \right|^2 = 0 \qquad (13)$$

due to the orthogonality of the signals with the noise subspace.

This is the important principle of null placement. The adaptive beamformer tries to place nulls in the beampattern in the direction of the interfering signals. This, of course, is how the minimum-energy beamformer minimizes output power. Note in figure 4 that the ME beampattern has a value of ~–66 dB at $\theta = 30°$. In fact, if the signals are of infinitely high SNR, the nulls will be perfect. The MUSIC beamformer, by excluding the signal space eigenvectors from its projection matrix

$$\sum_{i=K+1}^{N} \frac{1}{\lambda_i} \mathbf{v}_i \mathbf{v}_i^* ,$$

effectively increases the SNR of the signals and the nulls are perfect regardless.

IV. ADAPTIVE ARRAY RESPONSE AND APPROXIMATION

Next we will investigate the array response of the adaptive beamformers. Once again return to expression (8) for the minimum energy steering vector. With μ and the α_i's as before, we have

$$\mathbf{W}_{steer} = \mu \mathbf{R}^{-1} \mathbf{S}_{steer}$$

$$= \mu \left| \sum_{i=1}^{N} \frac{1}{\lambda_i} \mathbf{V}_i \mathbf{V}_i^* \right| \mathbf{S}_{steer}$$

$$= \frac{\mu}{\lambda_N} \sum_{i=1}^{N} \frac{\lambda_N}{\lambda_i} \alpha_i \mathbf{V}_i$$

$$= \frac{\mu}{\lambda_N} \left[\sum_{i=1}^{N} \frac{\lambda_N}{\lambda_i} \alpha_i \mathbf{V}_i - \sum_{i=1}^{N} \alpha_i \mathbf{V}_i + \mathbf{S}_{steer} \right]$$

$$= \frac{\mu}{\lambda_N} \left[\mathbf{S}_{steer} - \sum_{i=1}^{N} \frac{\lambda_i - \lambda_N}{\lambda_i} \alpha_i \mathbf{V}_i \right]. \tag{14}$$

If the signal plus noise field is that described by (6), then we can take advantage of the multiplicity of the smallest eigenvalue ($\lambda_{K+1} = \lambda_{K+2} = \ldots = \lambda_N = \sigma_n^2$) to write

$$\mathbf{W}_{steer} = \frac{\mu}{\sigma_n^2} \left[\mathbf{S}_{steer} - \sum_{i=1}^{K} \frac{\lambda_i - \sigma_n^2}{\lambda_i} \alpha_i \mathbf{V}_i \right]. \tag{15}$$

Also, the K largest eigenvectors span the signal space. With $\mathbf{S}_i$ representing the i^{th} unit norm plane-wave signal (i = 1,2, ..., K), we can perform a change of basis and write

$$\mathbf{W}_{steer} = \frac{\mu}{\sigma_n^2} \left[\mathbf{S}_{steer} - \sum_{i=1}^{K} \mathbf{W}_i \mathbf{S}_i \right] \tag{16}$$

where the $\mathbf{W}_i$'s are (as yet undetermined) complex weights.

We proceed to derive an approximation for the adaptive array response in a field of K discrete signals and uncorrelated noise of power σ_n^2. Since $\mathbf{W}_{steer} = \mu \mathbf{R}^{-1} \mathbf{S}_{steer}$, we see that

$$\mathbf{R}^{-1} \mathbf{S}_{steer} = \frac{1}{\sigma_n^2} \left[\mathbf{S}_{steer} - \sum_{i=1}^{K} \mathbf{W}_i \mathbf{S}_i \right]$$

The output power of the minimum-energy (ME) beamformer is then given by

$$P_{ME} = \frac{1}{\mathbf{S}^*_{steer}\mathbf{R}^{-1}\mathbf{S}_{steer}}$$

$$= \frac{1}{\mathbf{S}^*_{steer}\left(\frac{1}{\sigma_n^2}\left(\mathbf{S}_{steer} - \sum_{i=1}^{K} W_i S_i\right)\right)}$$

$$= \frac{\sigma_n^2}{1 - \sum_{i=1}^{K} W_i \mathbf{S}^*_{steer}\mathbf{S}_i} \quad . \tag{17}$$

The output power of the MUSIC beamformer is given by

$$P_{MUSIC} = \frac{1}{\mathbf{S}^*_{steer}\left(\sum_{i=K+1}^{N} \frac{1}{\lambda_i}\mathbf{V}_i\mathbf{V}_i^*\right)\mathbf{S}_{steer}} \quad .$$

In a similar fashion, we derive:

$$P_{MUSIC} = \frac{1}{\mathbf{S}^*_{steer}\left(\frac{1}{\sigma_n^2}\left(\sum_{i=K+1}^{N} \frac{\sigma_n^2}{\lambda_i}\alpha_i\mathbf{V}_i + \mathbf{S}_{steer} - \sum_{i=1}^{N} \alpha_i\mathbf{V}_i\right)\right)}$$

$$\text{with } \alpha_i = \mathbf{V}_i^*\mathbf{S}_{steer}$$

$$= \frac{1}{\mathbf{S}_{steer}\left(\frac{1}{\sigma_n^2}\left(\mathbf{S}_{steer} - \sum_{i=1}^{K} \alpha_i\mathbf{V}_i\right)\right)}$$

$$= \frac{\sigma_n^2}{1 - \sum_{i=1}^{K} W_i \mathbf{S}^*_{steer}\mathbf{S}_i} \quad ,$$

Which is the same as equation (17).

One way to evaluate the weights W would be to calculate the eigenvectors and eigenvalues of **R** and, given the signal vector S_j, change bases from (15) to (16). This would be cumbersome, however, and little insight would be gained. Therefore, we take another tack. For any given steering direction S_{steer}, we require that perfect nulls be placed in the adaptive beampattern in the direction of each of the K discrete signals. That is, we require that

$$\left| W^*_{steer} S_j \right|^2 = \left| \frac{\mu}{\sigma_n^2} \left(S^*_{steer} S_j - \sum_{L=1}^{K} W_i^* S_i^* S_J \right) \right|^2 = 0$$

for j = 1,2, ..., K. This gives rise to a system of equations:

$$\begin{bmatrix} 1 & S_1^* S_2 & \cdots & S_1^* S_K \\ S_2^* S_2 & 1 & \ddots & \\ S_K^* S_1 & \cdot & \cdots & 1 \end{bmatrix} \begin{bmatrix} W_1 \\ W_2 \\ \vdots \\ W_K \end{bmatrix} = \begin{bmatrix} S_1^* S_{steer} \\ S_2^* S_{steer} \\ \vdots \\ S_K^* S_{steer} \end{bmatrix} \tag{18}$$

In another notation:

$$A^* A \cdot \begin{bmatrix} W_1 \\ W_2 \\ \vdots \\ W_K \end{bmatrix} = A^* S_{steer} \tag{19}$$

where **A** is the N x K matrix whose columns are the signal vectors, as before. The weights are, thus, a function of steering angle and are related to the conventional beampatterns.

With the weights from (19), the minimum energy and MUSIC response plots are approximated by

$$P_{ABF} \simeq \frac{\sigma_n^2}{1 - S^*_{steer} A (A^* A)^{-1} A^* S_{steer}} \tag{21}$$

Looking at **A*A** in expression (18), we see that if the signal vectors are mutually orthogonal, the cross terms are zero and we have the result that $W_i = S_i^* S_{steer}$. In general, they are not. The $S_i^* S_j$ represent sidelobe levels in the conventional beampatterns. Provided the source arrival directions are greater than a beamwidth apart, however, the magnitude of the cross terms is small. The terms are small in the same sense that interelement correlations in isotropic noise are small if elements are a correlation length apart. Thus, we assume that $A^* A$ is a diagonally dominant matrix and $(A^* A)^{-1} \simeq I$.

Finally, we have an approximation for the adaptive array response (valid in the side-lobe region):

$$P_{ABF} \simeq \frac{\sigma_n^2}{1 - \sum_{i=1}^{K} |S_i^* S_{steer}|^2} \quad . \tag{22}$$

This relates the adaptive array response to the conventional beampatterns steered at each of the discrete signals.

V. VALIDATION OF APPROXIMATION

In a series of simulations, expression (22) was validated. Figures 6 through 19 show plots of the actual ME array response and the adaptive beamforming (ABF) approximation (22) for the 20-element half-wavelength line array of figure 5. Two signal plus noise fields were used. In the first, a single 20-dB SNR signal was present at $\theta = 30°$ in uncorrelated noise. For the second, three 20-dB SNR signals were present at $\theta = 30°$, 90°, and 135°. Included in the plots are some conventional beampatterns steered at discrete signals normalized to the output power in the direction of the signals. Also included are details of the array-response pattern in the sidelobe region. Notice in figure 7 the high level of agreement between the actual ME array response and our ABF approximation. Also note how closely the ABF response resembles a scaled version of the conventional beampattern of figure 6. MUSIC beamformer array-response plots are not shown in this series, but it was found that MUSIC array responses were nearly identical to ME array responses in the sidelobe region.

Figures 10 and 11 are a set of plots for a 20-element quarter-wavelength line array in the second noise field. Here we also see good agreement between the actual ME array response and the approximation. Figures 12 through 16 comprise another set with the same noise fields and the 17-element Mill's cross array (figure 1).

Of particular interest is figure 15. A high spurious peak in the array-response plot occurs at $\simeq\theta = 270°$. The approximation appears higher than the actual peak here. We also see in this figure that the conventional beampattern steered at the second signal ($\theta = 90°$) has a high sidelobe at $\theta = 270°$. This sidelobe manifests itself as a high peak in the array-response plot at that location. Thus, this peak is a characteristic of the array and not of the noise field.

The final array type used in this series was a random planar array in which the elements were distributed uniformly on a circle. Figure 17 shows a random circle of diameter 6 wavelengths. The conventional beampatterns in the plots which follow show a much different structure than those of the line arrays or the deterministic Mill's cross array. The patterns are much less regular and the sidelobes less pronounced. This is a characteristic of random arrays. Figures 18 through 21 are in a series identical to those previous for the random circle.

It is instructive to review the assumptions which led to expression (22), an approximation for the ABF array response in the region away from the signals. The first was that the signal plus noise field consists of K signals in uncorrelated noise of power σ_n^2. The second was that the nulls in the beampatterns are perfect. The third was that $(\mathbf{A}^*\mathbf{A})^{-1} \simeq \mathbf{I}$. This last is most open to question. For one thing, expression (22) now has a singularity wherever

$$\sum_{i=1}^{K} |\mathbf{S}_i^* \mathbf{S}_{steer}|^2 \geq 1 \text{ (generally near the signals).}$$

As a bound on $||(\mathbf{A}^*\mathbf{A})^{-1} - \mathbf{I}||$, we have

$$||\mathbf{I} - (\mathbf{A}^*\mathbf{A})^{-1}|| \leq \frac{||\mathbf{I} - \mathbf{A}^*\mathbf{A}||}{1 - ||\mathbf{I} - \mathbf{A}^*\mathbf{A}||} \tag{23}$$

(Appendix I). As a typical value for $||\mathbf{I} - \mathbf{A}^*\mathbf{A}||$ consider that for a random array, $|\mathbf{S}_i^*\mathbf{S}_j|^2$ are random variables with mean $1/N$ and variance $1/N^2$ provided the signals are greater than a beamwidth apart. Then,

$$||\mathbf{I} - \mathbf{A}^*\mathbf{A}|| = \sqrt{\frac{1}{K} \sum_{\substack{i=1 \\ i \neq j}}^{K} \sum_{j=1}^{K} |\mathbf{S}_i^*\mathbf{S}_j|^2}$$

$$\simeq \sqrt{\frac{k^2 - K}{K} \cdot \frac{1}{N}} = \sqrt{\frac{K - 1}{N}} \quad ,$$

and

$$||\mathbf{I} - (\mathbf{A}^*\mathbf{A})^{-1}|| \leq \frac{\sqrt{\frac{K - 1}{N}}}{1 - \sqrt{\frac{K - 1}{N}}} \quad .$$

For $K = 3$ and $N = 20$, this value is $\simeq .46$.

We can rewrite expression (22)

$$P_{ABF} \simeq \frac{\sigma_n^2}{1 - \sum_{i=1}^{K} |\mathbf{S}_i^*\mathbf{S}_{steer}|^2}$$

by writing it as a geometric series:

$$P_{ABF} \simeq \sigma_n^2 \left[1 + \sum_{i=1}^{K} |\mathbf{S}_i^*\mathbf{S}_{steer}|^2 + \left(\sum_{i=1}^{K} |\mathbf{S}_i^*\mathbf{S}_{steer}|^2 \right)^2 + \cdots \right] .$$

This could be truncated for small $\Sigma|\mathbf{S}_i^*\mathbf{S}_{steer}|^2$ to

$$P_{ABF} \simeq \sigma_n^2 \left[1 + \sum_{i=1}^{K} |\mathbf{S}_i^*\mathbf{S}_{steer}|^2 \right] . \qquad (24)$$

This is very similar to expression (7) for the conventional beamformer output power. Regardless of how we express it, however, it is clear that the adaptive beamformer, as well as the conventional, has a spatial spectrum which is dependent on the term $\sum_{i=1}^{K} |\mathbf{S}_i^*\mathbf{S}_{steer}|^2$.

VI. AN EXAMPLE USING A RANDOMIZED ARRAY

A particularly dramatic example of the impact of $|S_i^* S_{steer}|^2$ on the adaptive beamformer is shown in the following series of plots. Figure 22 is of a 20-element rectangular array. Figure 23 shows the conventional beampattern steered at $\theta = 15°$. There is an exceptionally high sidelobe at $\simeq\theta = 167°$. Figure 24 shows the ME array response of this array to a signal plus noise field consisting of a single 0-dB SNR signal at $\theta = 15°$ in uncorrelated noise. The tremendous (about 7.5 dB) spurious peak at $\simeq\theta = 167°$ arises from the array. It would certainly be counted as a false detection if not recognized as such.

As previously suggested in comments on the random circular array, beampatterns of random arrays fail to display to extremely high sidelobes which arise due to the symmetries in most deterministic arrays. By randomizing an array (i.e., adding a random component to the element position vectors) peak sidelobes can be reduced. The effect on signal detection is that spurious peak levels are decreased.

With this in mind, the deterministic positions $\mathbf{Z} = \begin{bmatrix} x \\ y \end{bmatrix}$ of the rectangular array of figure 22 were perturbed by $\begin{bmatrix} \tilde{x} \\ \tilde{y} \end{bmatrix}$. The $\tilde{x}$ and $\tilde{y}$ random variables (measured in wavelengths) were selected uniformly on the interval $[-\epsilon/2, +\epsilon/2]$. Selection of the parameter ϵ allows one to move between the deterministic array ($\epsilon = 0$) and the totally random array ($\epsilon \simeq .5$ in this case). Figure 25 through 27 show the conventional beampatterns steered to $\theta = 15°$ as the randomization parameter ϵ is increased from 0.1 to 0.5. For small perturbation ($\epsilon = 0.1, 0.3$), the peak at $\theta = 167°$ is still present although with somewhat less magnitude. At higher values ($\epsilon = 0.4, \ldots$), the array is, effectively, totally random and the deterministic peak is submerged in the random pattern.

Figures 28 through 30 show the corresponding ME array-response plots. For the deterministic and slightly randomized arrays, the spurious peak is pronounced but decreases rapidly as the array is more random. Figure 31 displays graphically the correspondence between peak sidelobe level (in the conventional beampattern) and peak spurious peak level (in the array response). It also displays the effectiveness of using randomization to decrease both.

VII. SPURIOUS PEAK ESTIMATOR FOR RANDOM ARRAYS

For an array in which the element position vectors are random, the quantity

$$|S_1^* S_{steer}|^2 \equiv b = \frac{1}{N^2} \sum_{n=1}^{N} \sum_{m=1}^{N} e^{i \frac{\omega}{c} (\kappa_1 - \kappa_{steer}, Z_n - Z_m)} \tag{25}$$

is a random variable provided S_1 and S_{steer} are greater than a beamwidth apart. It has a probability density function given by

$$f(b) = \frac{1}{\sigma^2} e^{-b/\sigma^2} \; ; \; b \geq 0 \tag{26}$$

where $\sigma^2 \equiv 1/N$ (Steinberg, 1976, eq. 8.18). This density has mean $1/N$ and variance $1/N^2$ and represents the probability that the sidelobe level will attain a certain value.

If we assume that the beampatterns are independent of each other, then the sum

$$y = \sum_{i=1}^{K} |S_i^* S_{steer}|^2$$

has a probability density function g(y) given by

$$g(y) = \frac{1}{(K-1)!(\sigma^2)^K} y^{K-1} e^{-y/\sigma^2} \; ; \; y \geq 0 \text{ (Appendix 2)} . \tag{27}$$

The output power of the adaptive beamformer for a random array is, thus, a random variable in the region away from the signals. The transformation is

$$P_{ABF} \simeq \frac{\sigma_n^2}{1 - \sum_{i=1}^{K} |S_i^* S_{steer}|^2} = \frac{\sigma_n^2}{1 - y} .$$

The probability that y is greater than or equal to 1 and tne output power is infinite away from any of the signals is

$$e^{-1/\sigma^2} \left[1 + \frac{1}{\sigma^2} + \frac{1}{2!} \left(\frac{1}{\sigma^2} \right) + \ldots + \frac{1}{(K-1)!} \left(\frac{1}{\sigma^2} \right)^{K-1} \right] ,$$

which is negligible for most reasonable choices of K and $N > K$. The output power P_{ABF}, in the region away from the signals, has a probability density function h(p) given by

$$h(p) = \frac{\sigma_n^2}{p^2(K-1)!(\sigma^2)^k}\left[1 - \frac{\sigma_n^2}{p}\right]^{K-1} \exp\left[-\frac{1}{\sigma^2}\left(1 - \frac{\sigma_n^2}{p}\right)\right] ; \; p \geq \sigma_n^2 \quad (28)$$

and a distribution function

$$h(p) = \int_{\sigma_n^2}^{p} h(t)dt$$

$$= 1 - \exp\left[-\frac{1}{\sigma^2}\left(1 - \frac{\sigma_n^2}{p}\right)\right] \cdot \left[1 + \frac{1}{\sigma^2}\left(1 - \frac{\sigma_n^2}{p}\right) + \ldots\right.$$

$$\left. + \frac{1}{(K-1)!}\left(\frac{1}{\sigma^2}\left(1 - \frac{\sigma_n^2}{p}\right)\right)^{K-1}\right]. \quad (29)$$

We develop our estimate for a peak spurious peak in much the same way that Steinberg (1976) arrives at a peak sidelobe estimator. Since the beampatterns of an array are completely described by some number of independent samples n (determined from the correlation properties of the beampattern, and the array-response plot is a function of those beampatterns) it follows that the array-response pattern is described by n samples also.

For a random circular planar array of diameter D, the correlation structure is described by

$$\frac{2J_1\left(\frac{\pi D}{\lambda}u\right)}{\left(\frac{\pi D}{\lambda}u\right)}$$

where u is related to the angle between look directions γ by

$$u = \pm 2 \sin\left(\frac{1}{2}\gamma\right)$$

and j_1 is the first order Bessel function of the first kind. The number of independent samples or array parameter n is given by

$$n = \frac{\pi}{\sin^{-1}\left[.60984\,\frac{\lambda}{D}\right]} \quad . \tag{30}$$

The probability that a peak spurious peak will not exceed some threshold β is then given by

$$\Pr[\text{peak spurious peak} \leq \beta] = [H(\beta)]^n \quad , \tag{31}$$

where $H(\beta)$ and n are given by *(29) and (30).*

A number of 20-element random circular arrays of radius $D = 10\lambda$ were generated. In a noise field consisting of 0-dB white noise and three signals with various arrival and strength structure, minimum-energy array-response plots were calculated. In 50 trials, a peak spurious peak was found and a cumulative histogram of these values appears on figure 32. Also plotted is $[H(\beta)]^n$ against the threshold β in dB for the appropriate parameters.

$$n = \frac{\pi}{\sin^{-1}[.60984/10]} = 51$$

$$\sigma_n^2 = 1$$

$$\sigma^2 = \frac{1}{N} = \frac{1}{20}$$

$$K = \text{number of signals} = 3 \quad . \tag{32}$$

This shows remarkable agreement!

Figure 33 displays a series of $[H(\beta)]^n$ against β for a variety of 20-element random circle arrays. The signal plus noise field is assumed to consist of three signals in 0-dB uncorrelated noise. The independent variable is the array parameter n or, equivalently, the array size. For a fixed number of elements, an increase in diameter while decreasing mainlobe width (and thus increasing resolution capabilities) also has the effect of raising the probability of spurious peak threshold exceedance (thus, increasing the probability of false detections). Peak-sidelobe estimates for the same arrays are displayed in figure 34. The correspondence between peak sidelobes and peak spurious peaks is clear.

Figures 35 through 38 illustrate the ME array-response plots for some realizations of 20-element circular random arrays of various diameters. The signal plus noise field consists of three signals, 20-dB SNR at $\theta = 0°$, 10-dB SNR at $\theta = 45°$, and 0-dB SNR at $\theta = 90°$, in uncorrelated noise. Figure 35 also shows the MUSIC array response and the conventional array response. Note the appearance of spurious peaks away from the signals in the adaptive array responses.

For a random line array of length L, the correlation structure is described by

$$\frac{\sin\left(\frac{\pi L}{\lambda}u\right)}{\left(\frac{\pi L}{\lambda}u\right)}$$

where u is related to the steering angle θ measured from broadside by

$$u = \sin\theta - \sin\theta_o \ .$$

Here, θ_o is the steering angle. The array parameter n is

$$n = \frac{L}{\lambda}\left[1 + |\sin\theta_o|\right]$$

The array parameter is, thus, dependent on steering direction (or, in the context of signal detection, signal direction of arrival). Since the signals arrive from all directions, we require a representative value for n. For this we use

$$\bar{n} = \frac{L}{\lambda}\left[1 + \frac{1}{\pi}\int_{-\frac{\pi}{2}}^{+\frac{\pi}{2}} |\sin\theta| d\theta\right] = \frac{L}{\lambda}\left[1 + \frac{2}{\pi}\right]. \qquad (33)$$

Figure 39 displays $[H(\beta)]^{\bar{n}}$ against β for a 20-element line with three signals in 0-dB uncorrelated noise. The independent variable, as in the case of the circle array, is the array parameter or, equivalently, the line length. Figures 40 through 43 are representative ME array-response plots for random lines of various lengths. The signal plus noise field consists of a 20-dB SNR signal at $\theta = 0°$, a 10-dB SNR signal at $\theta = 45°$, and a 0-dB SNR signal at $\theta = 90°$. Figure 40 also displays the MUSIC beamformer and conventional array response.

VIII. DETECTION PROBABILITIES FOR MINIMUM-ENERGY PROCESSING WITH RANDOM ARRAYS

The peak spurious peak impacts the probability of detecting a weak signal in an obvious way. In this section, we evaluate the probability of detecting a signal when minimum energy processing is used with a random array.

Suppose that the noise field is described by a correlation matrix

$$\mathbf{R} = N\sigma_S^2\, \mathbf{S}_o\mathbf{S}_o^* + \mathbf{Q} \tag{34}$$

where $\mathbf{S}_o$ is the signal we are interested in detecting and $\mathbf{Q}$ describes the remainder of the noise field. In particular, suppose the background noise field consists of K interfering signals $\mathbf{S}_1, \ldots, \mathbf{S}_k$ of powers $\sigma_1^2, \ldots, \sigma_K^2$ respectively in uncorrelated noise of power σ_n^2. Then,

$$\mathbf{Q} = N\sigma_1^2\, \mathbf{S}_1\mathbf{S}_1^* + \ldots + N\sigma_K^2\, \mathbf{S}_k\mathbf{S}_k^* + \sigma_n^2\, \mathbf{I}\ . \tag{35}$$

Here we assume that the interest signal $\mathbf{S}_o$ is in the region away from the K interferers.

With $\mathbf{R}$ as described by (34), a useful fact is that

$$\mathbf{R}^{-1} = \mathbf{Q}^{-1} - \frac{\mathbf{Q}^{-1}\,\mathbf{S}_o\,\mathbf{S}_o^*\,\mathbf{Q}^{-1}}{\mathbf{S}_o^*\,\mathbf{Q}^{-1}\,\mathbf{S}_o + 1/N\sigma_S^2}\ .$$

The minimum-energy filter vector $\mathbf{W}_o$ when the array is stored in the direction of the signal $\mathbf{S}_o$ is then

$$\mathbf{W}_o = \frac{\mathbf{R}^{-1}\,\mathbf{S}_o}{\mathbf{S}_o^*\,\mathbf{R}^{-1}\,\mathbf{S}_o}$$

$$= \frac{\left[\mathbf{Q}^{-1} - \dfrac{\mathbf{Q}^{-1}\,\mathbf{S}_o\,\mathbf{S}_o^*\,\mathbf{Q}^{-1}}{\mathbf{S}_o^*\,\mathbf{Q}^{-1}\,\mathbf{S}_o + 1/N\sigma_S^2}\right]\mathbf{S}_o}{\mathbf{S}_o^*\left[\mathbf{Q}^{-1} - \dfrac{\mathbf{Q}^{-1}\,\mathbf{S}_o\,\mathbf{S}_o^*\,\mathbf{Q}^{-1}}{\mathbf{S}_o^*\,\mathbf{Q}^{-1}\,\mathbf{S}_o + 1/N\sigma_S^2}\right]\mathbf{S}_o}$$

$$= \frac{\mathbf{Q}^{-1}\,\mathbf{S}_o - \dfrac{\mathbf{Q}^{-1}\,\mathbf{S}_o\,\mathbf{S}_o^*\,\mathbf{Q}^{-1}\,\mathbf{S}_o}{\mathbf{S}_o^*\,\mathbf{Q}^{-1}\,\mathbf{S}_o + 1/N\sigma_S^2}}{\mathbf{S}_o^*\,\mathbf{Q}^{-1}\,\mathbf{S}_o - \dfrac{\mathbf{S}_o^*\,\mathbf{Q}^{-1}\,\mathbf{S}_o\,\mathbf{S}_o^*\,\mathbf{Q}^{-1}\,\mathbf{S}_o}{\mathbf{S}_o^*\,\mathbf{Q}^{-1}\,\mathbf{S}_o + 1/N\sigma_S^2}}$$

$$= \frac{\mathbf{Q}^{-1}\mathbf{S}_o}{\mathbf{S}_o^* \mathbf{Q}^{-1}\mathbf{S}_o} \left[\frac{1 - \dfrac{\mathbf{S}_o^* \mathbf{Q}^{-1}\mathbf{S}_o}{\mathbf{S}_o^* \mathbf{Q}^{-1}\mathbf{S}_o + 1/N\sigma_S^2}}{1 - \dfrac{\mathbf{S}_o^* \mathbf{Q}^{-1}\mathbf{S}_o}{\mathbf{S}_o^* \mathbf{Q}^{-1}\mathbf{S}_o + 1/N\sigma_S^2}} \right]$$

$$= \frac{\mathbf{Q}^{-1}\mathbf{S}_o}{\mathbf{S}_o^* \mathbf{Q}^{-1}\mathbf{S}_o} \quad .$$

Hence, the output power of the ME beamformer in the direction of the signal of interest is

$$P_{ME} = \mathbf{W}_o^* \mathbf{R} \mathbf{W}_o$$

$$= \frac{\mathbf{S}_o^* \mathbf{Q}^{-1}}{\mathbf{S}_o^* \mathbf{Q}^{-1}\mathbf{S}_o} \left[N\sigma_S^2 \mathbf{S}_o \mathbf{S}_o^* + \mathbf{Q} \right] \frac{\mathbf{Q}^{-1}\mathbf{S}_o}{\mathbf{S}_o^* \mathbf{Q}^{-1}\mathbf{S}_o}$$

$$= N\sigma_S^2 + \frac{1}{\mathbf{S}_o^* \mathbf{Q}^{-1}\mathbf{S}_o} \quad . \tag{36}$$

Since Q contains no signals in the direction of S_o, our earlier sidelobe approximation is valid for the second term in (36). Writing

$$y = \frac{1}{\mathbf{S}_o^* \mathbf{Q}^{-1}\mathbf{S}_o} \quad ,$$

we have that

$$y \simeq \frac{\sigma_n^2}{1 - \sum_{L=1}^{K} |\mathbf{S}_o^* \mathbf{S}_o|^2} \quad .$$

If the array is random, y is a random variable with a probability density function

$$h(y) = \frac{\sigma_n^2}{y^2 (k-1)! (\sigma^2)^K} \left[1 - \frac{\sigma_n^2}{y} \right]^{K-1} \exp\left[-\frac{1}{\sigma^2} \left(1 - \frac{\sigma_n^2}{y} \right) \right]$$

$$; \; y \geq \sigma_n^2 \quad . \tag{37}$$

This is just equation (28) with y in place of p. The output power p in the direction of the interest signal S_o is then $N\sigma_S^2 + y$ and is a random variable with a probability density function

$$j(p) = \frac{\sigma_n^2}{(p - N\sigma_n^2)^2(K-1)!(\sigma^2)^K}\left[1 - \frac{\sigma_n^2}{p - N\sigma_S^2}\right]^{K-1}$$

$$\cdot \exp\left[-\frac{1}{\sigma^2}\left(1 - \frac{\sigma_n^2}{p - N\sigma_S^2}\right)\right]; \; p \geq N\sigma_n^2 + \sigma_n^2 \; . \tag{38}$$

There are K + 1 signals in the noise field counting the interferers and the signal of interest. In the region away from any of these signals, the array-response level is a random variable with a probability density function similar to h(y) only with K + 1 replacing K. It is

$$\ell(y) = \frac{\sigma_n^2}{y^2 K!\,(\sigma^2)^{K+1}}\left[1 - \frac{\sigma_n^2}{y}\right]^K \exp\left[-\frac{1}{\sigma^2}\left(1 - \frac{\sigma_n^2}{y}\right)\right]; \; y \geq \sigma_n^2 \; ,$$

and the corresponding distribution function is

$$L(y) = \int_{\sigma_n^2}^{y} \ell(t)dt$$

$$= 1 - \exp\left[-\frac{1}{\sigma^2}\left(1 - \frac{\sigma_n^2}{y}\right)\right] \cdot \left[1 + \frac{1}{\sigma^2}\left(1 - \frac{\sigma_n^2}{y}\right)\right.$$

$$\left. + \ldots + \frac{1}{K!}\left(\frac{1}{\sigma^2}\left(1 - \frac{\sigma_n^2}{y}\right)\right)^K\right] \; . \tag{39}$$

Compare this with equation (28).

As presented in the previous section, the peak spurious peak is the largest of the n independent samples of the array-response pattern where n is the array paramcter. It is a random variable. Let r represent the level of the peak spurious peak and m(r) be its probability density function. The density m(r) is unknown, but the distribution function M(r) is found to be

$$M(r) = \int_{\sigma_n^2}^{r} m(t)dt = \left[L(r)\right]^n \; . \tag{40}$$

See equation (31).

For probability of signal detection, we take the probability that the signal peak p will exceed the peak spurious peak r. Assuming that p and r are independent, this is

$$\Pr[p > r] = \iint_{p>r} j(p)n(p)\,dr\,dp$$

$$= \int_{N\sigma_S^2 + \sigma_n^2}^{\omega} \left[\int_{\sigma_n^2}^{p} m(r)\,dr \right] j(p)\,dp$$

$$= \int_{N\sigma_S^2 + \sigma_n^2}^{\omega} M(p)j(p)\,dp$$

$$= \int_{N\sigma_S^2 + \sigma_n^2}^{\omega} [L(p)]^n\, j(p)\,dp \qquad (41)$$

where j(p) is given by (38) and L(p) by (39).

Making the substitution $\sigma^2 = 1/N$ and the change of variables $x = 1/\sigma^2 (1 - \sigma_n^2/p)$, this integral becomes

$$\Pr[p > r] = \int_{N\sigma_S^2 + \sigma_n^2}^{\omega} [L(p)]^n\, j(p)\,dp$$

$$= \int_{N\left(\frac{\delta}{\delta+1}\right)}^{N} \left\{ \left(1 - e^{-x} \left[1 + x + \ldots + \frac{x^k}{k!} \right] \right)^n \right.$$

$$\frac{N^2}{(N - \delta(N - x))^2 (K-1)!} \left[N \left(\frac{(\delta+1)x - N\delta}{\delta x + (1-\delta)N} \right) \right]^{K-1}$$

$$\left. \cdot \exp\left[- N \left(\frac{(\delta+1)x - N\delta}{\delta x + (1-\delta)N} \right) \right] \right\} dx$$

with $\delta = N\sigma_S^2/\sigma_n^2$. This integral was evaluated numerically.

Figure 44 is a plot of this probability against input SNR (σ_S^2/σ_n^2) for N = 20, n = 51, and K = 2. This corresponds to signal detection with a 20-element random circular array of diameter D = 10 λ in the presence of two interferers.

Following figure 44 is a series of plots displaying precisely this situation. A series of 20-element random circular planar arrays were generated. The "background" noise field consists of 0-dB white noise and two interferers. The interferers are located at θ = 45° and 90° and each has a SNR of 3 dB. The signal of interest — the one we want to detect — is located at θ = 180°.

In figure 45, the signal of interest has a SNR of -10 dB. Referring to figure 44, we see that, at this SNR, there is an extremely high probability that the signal peak will exceed the peak spurious peak. Indeed, the signal of interest is easily detected using minimum energy processing.

In figures 46 through 48, the interest signal has a SNR of -13.2 dB. At this source level, the probability is $\simeq$ .9 that the signal peak will exceed the peak spurious peak. For these three random arrays at this source level, the signal is easily detected as we would expect.

In figures 49 through 51, the interest signal has a SNR of -15.5 which corresponds to a probability of $\simeq$ .5. Here, we see that the signal is being lost in the side region noise. In figure 49, the signal peak is about equal in height to the peak spurious peak. In figure 50, for another realization of the random array, the signal peak is the highest peak. In figure 51, the signal is clearly lost in the noise.

The final figure of this series, figure 52, shows the minimum-energy array response for this noise field and a representative array when the SNR of the interest signal is -18.0 dB. This corresponds to a probability of $\simeq$ .1 and, as expected, the signal is lost in the noise.

Figures 53 and 54 are similar to figure 44. Both show the probability that the signal peak exceeds the peak spurious peak (i.e., the detection probability) for 20-element random arrays against input SNR. The first, figure 53, is for a noise field containing two interferers. Curves (left to right) are for n = 31, 41, 51, 71, 82, and 103 corresponding to circular planar arrays of diameters D = 6λ, 8λ, 10λ, 14λ, 16λ, and 20λ respectively. Note that for a fixed number of elements, increasing the physical size of the array decreases the probability of signal detection.

Figure 54 is for a noise field containing three interferes. Curves (left to right) correspond to array diameters of 6λ, 8λ, 10λ, 14λ, and 20λ. Comparing figures 53 and 54, we see that increasing the number of interferers complicates the noise field and, consequently, the array-response pattern making detection of weak signals more difficult.

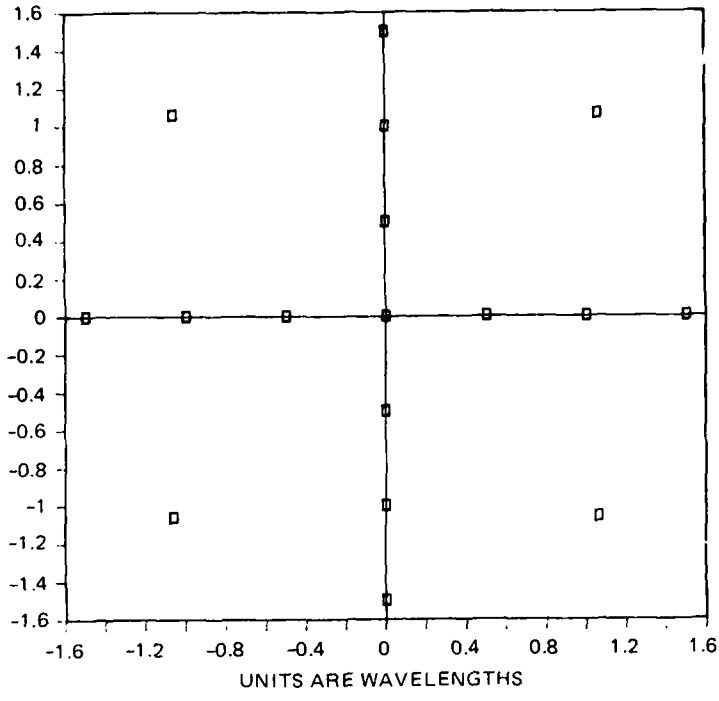

Figure 1. Mill's cross array. 17-element; half-wavelength.

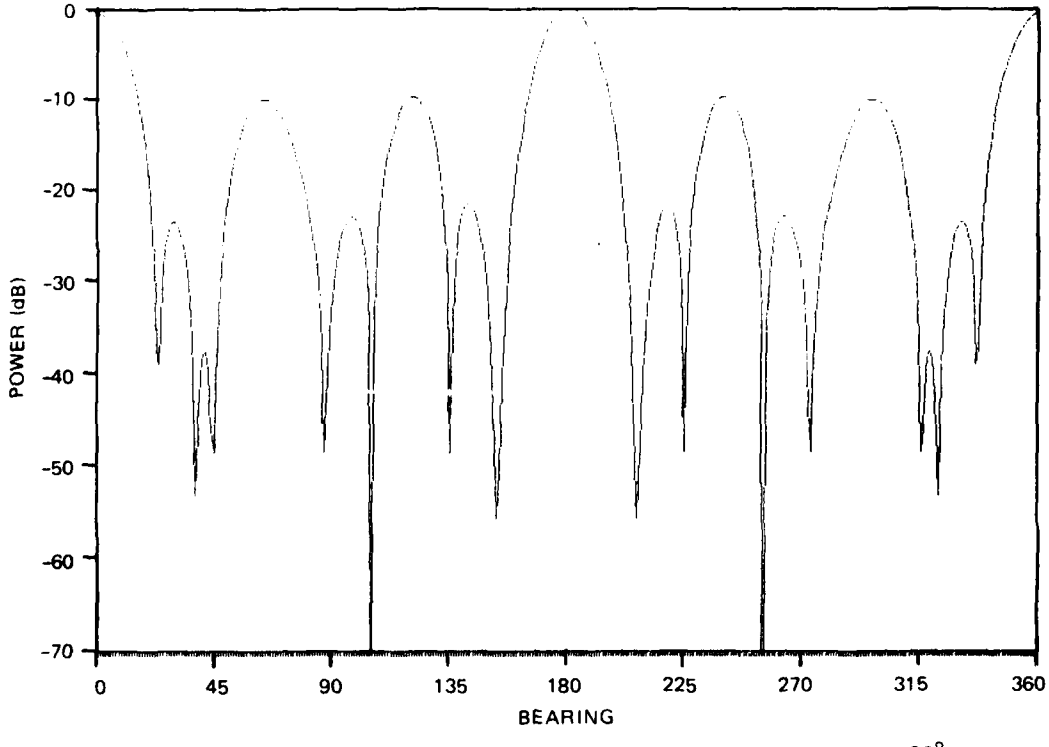

Figure 2. Conventional beampattern. Mill's cross array; steered at 180°.

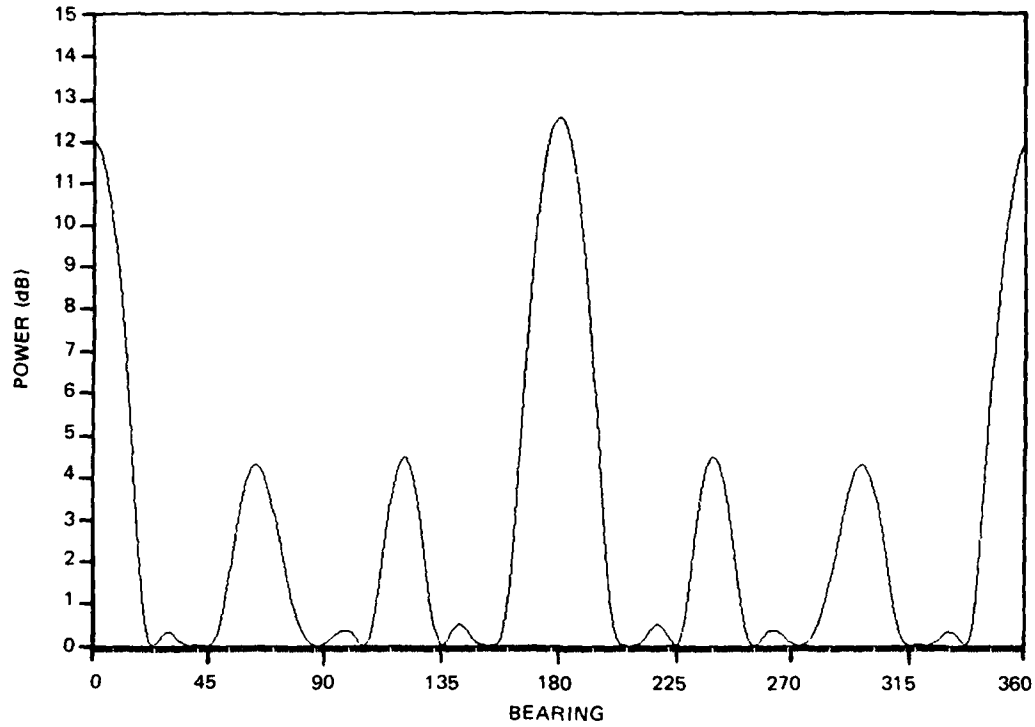

Figure 3. Conventional array response. Mill's cross array; one 0-dB SNR signal at 180°.

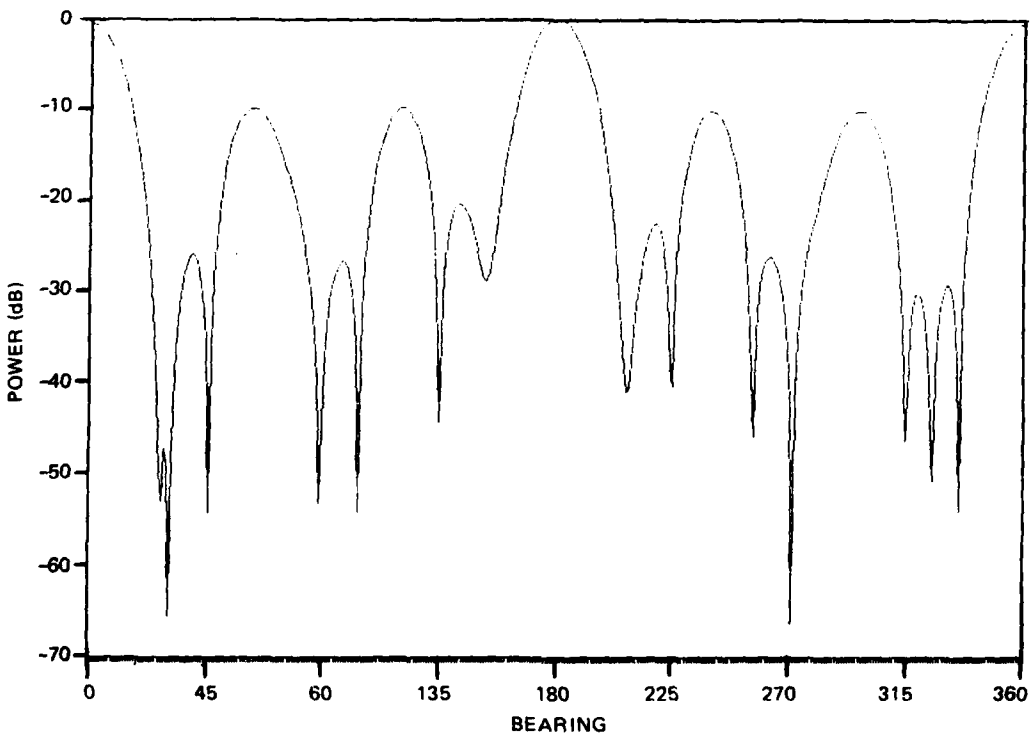

Figure 4. Adaptive ME beampattern. Mill's cross array; steered 180°, one signal at 30°.

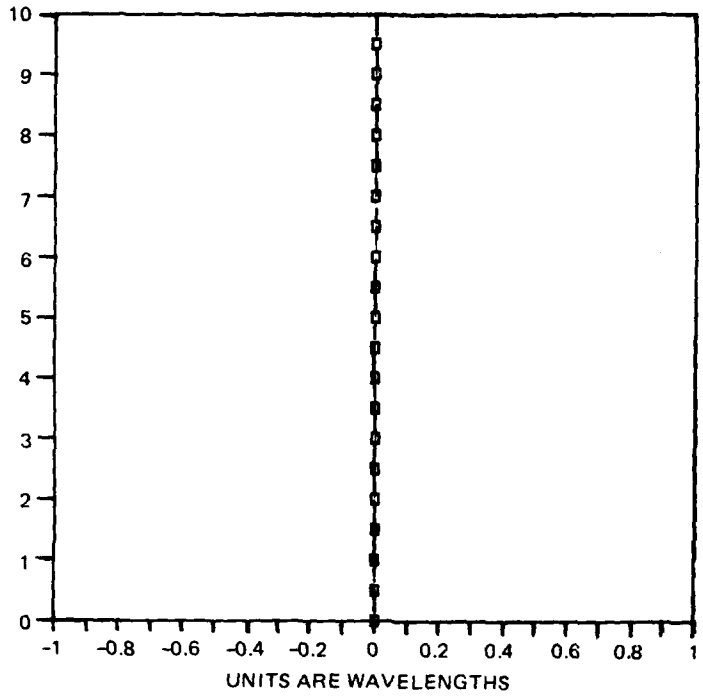

Figure 5. Line array. 20-element; half-wavelength spacing.

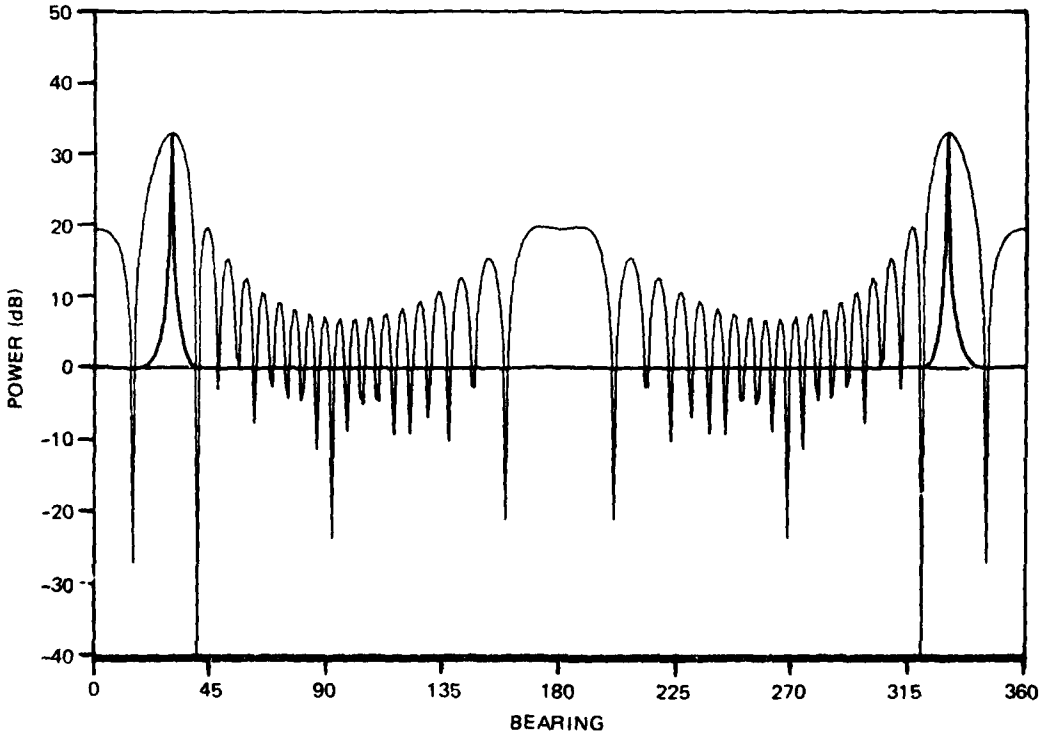

Figure 6. MAR and CBP. 20-element line; half-wavelength.

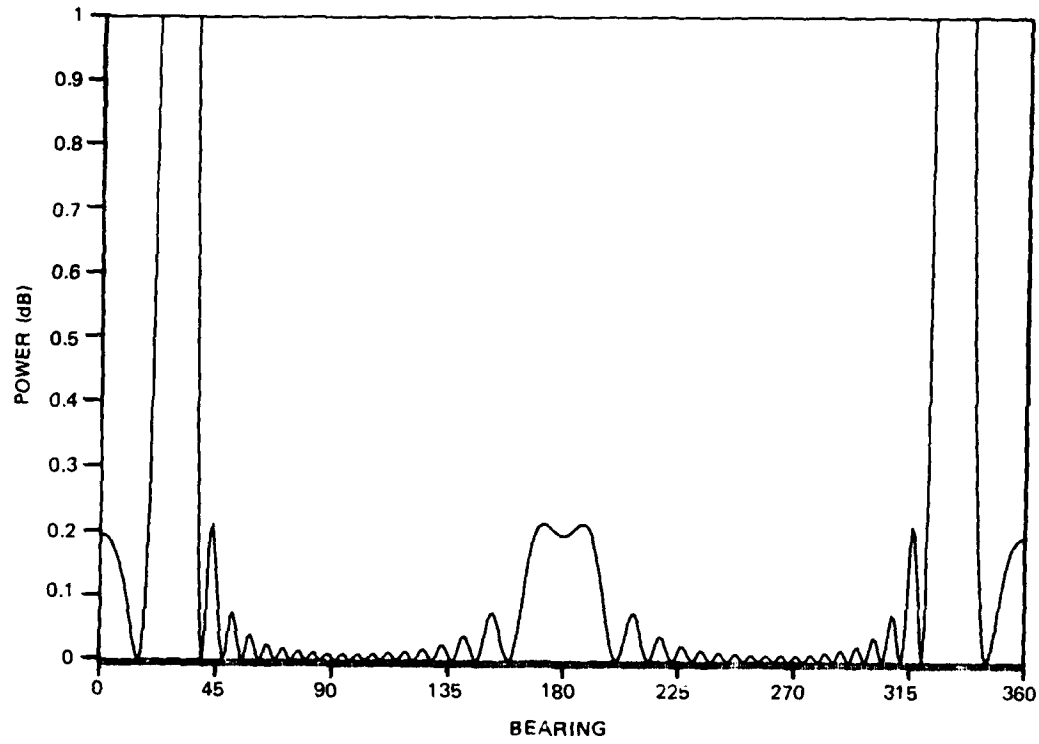

Figure 7. AAR detail. 20-element line; half-wavelength.

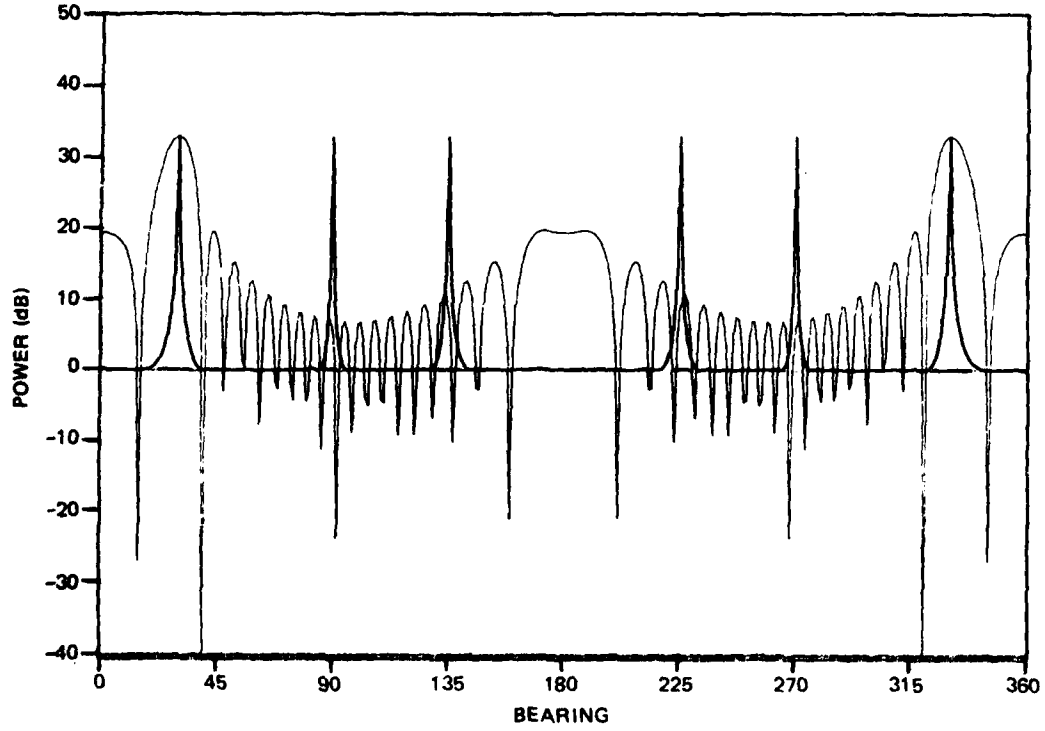

Figure 8. AAR and CBP. 20-element line; half-wavelength.

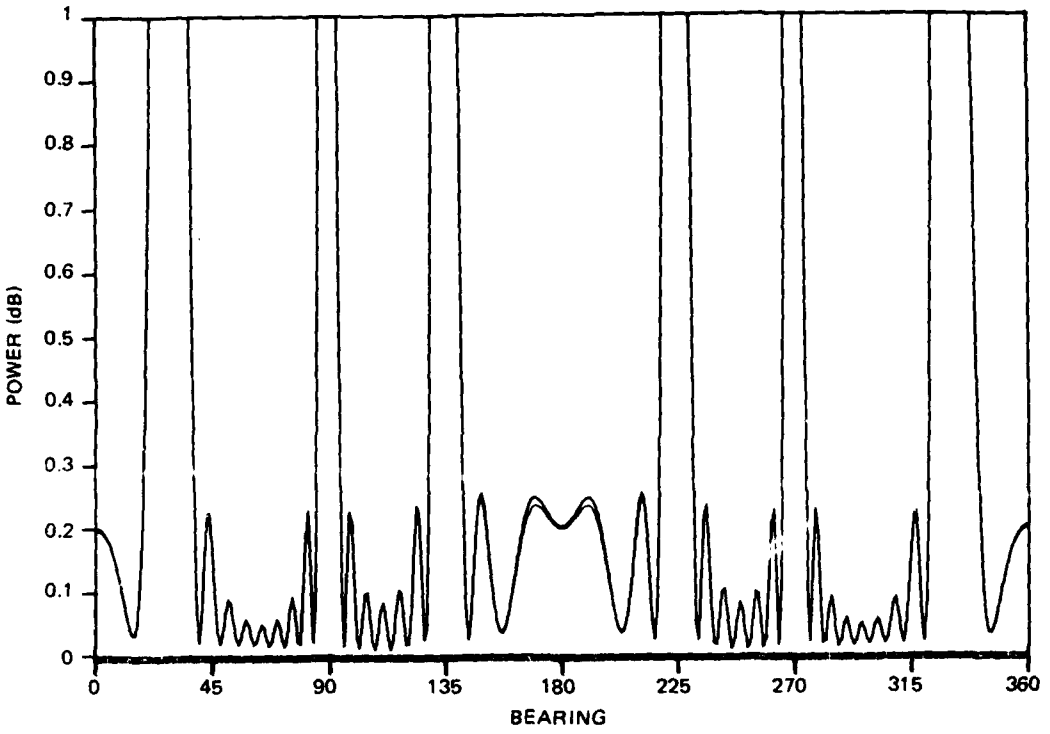

Figure 9. AAR detail. 20-element line; half-wavelength.

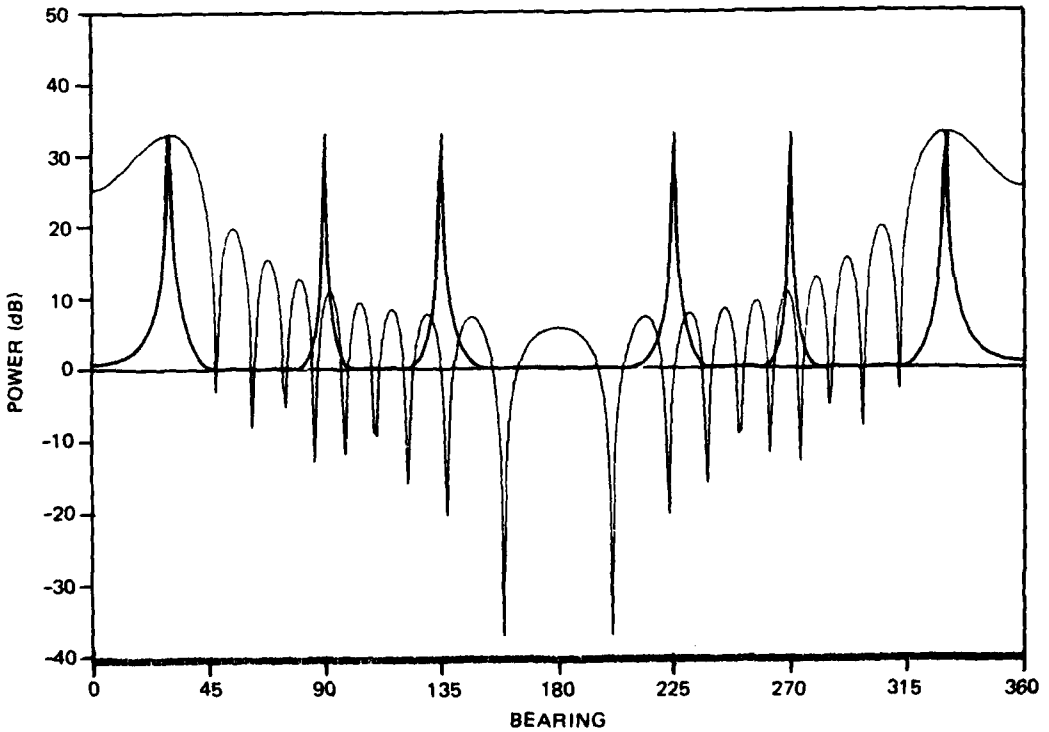

Figure 10. AAR and CBP. 20-element line; quarter-wavelength.

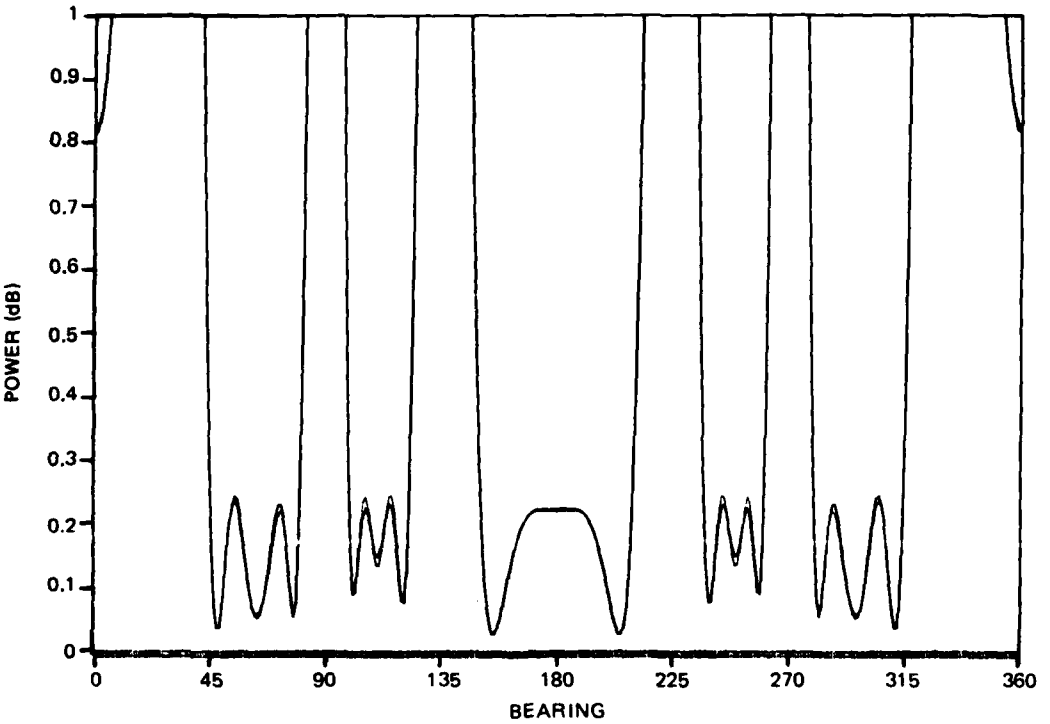

Figure 11. AAR detail. 20-element line; quarter-wavelength.

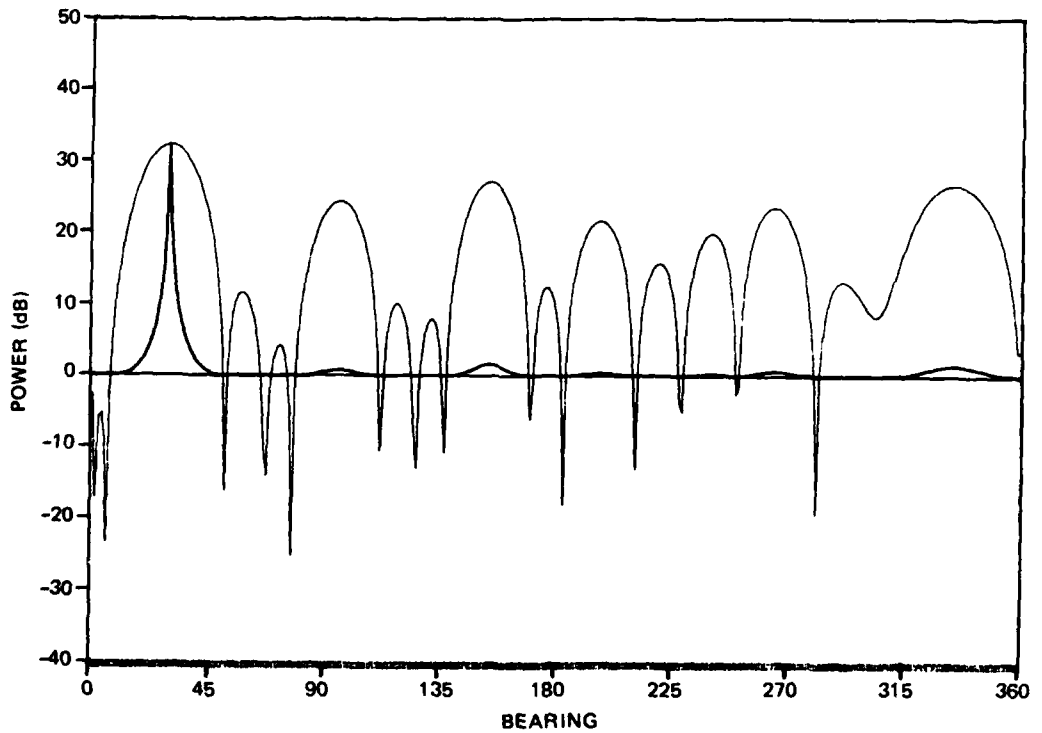

Figure 12. AAR and CBP. Mill's cross array; half-wavelength.

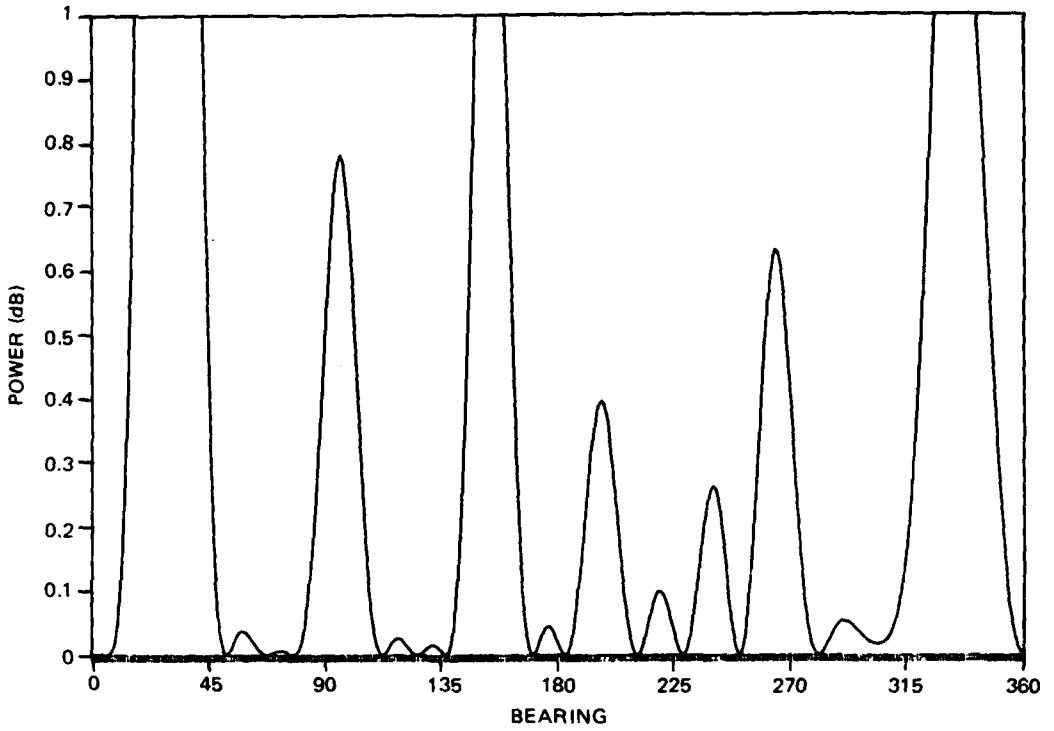

Figure 13. AAR detail. Mill's cross array; half-wavelength.

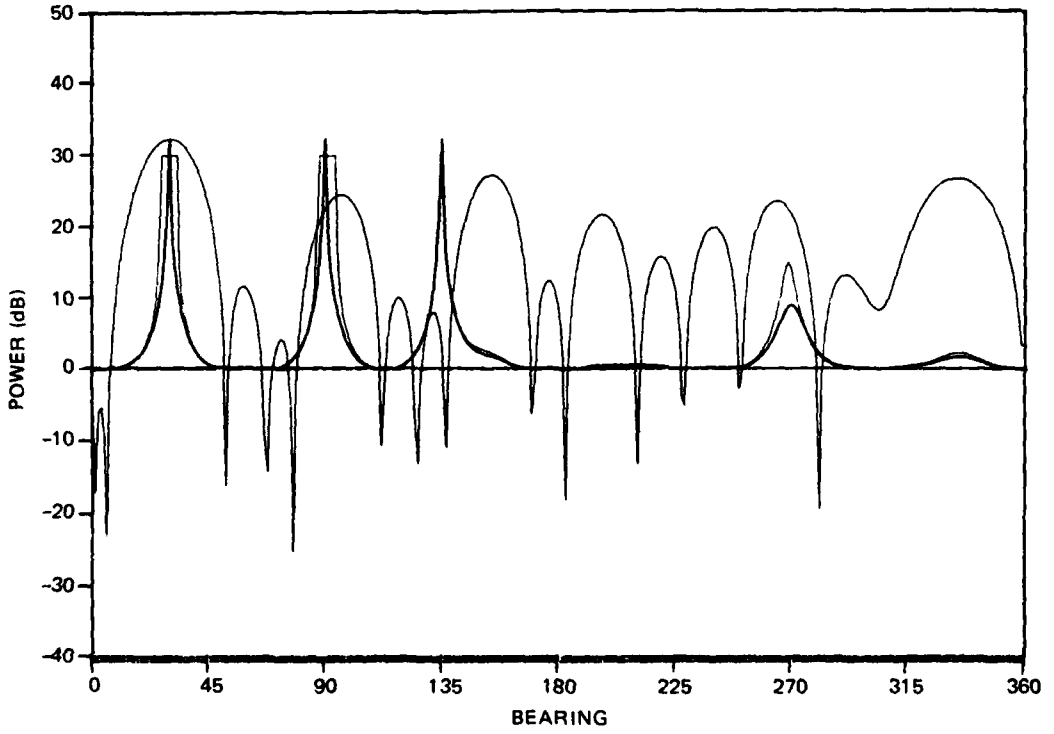

Figure 14. AAR and CBP. Mill's cross array: half-wavelength.

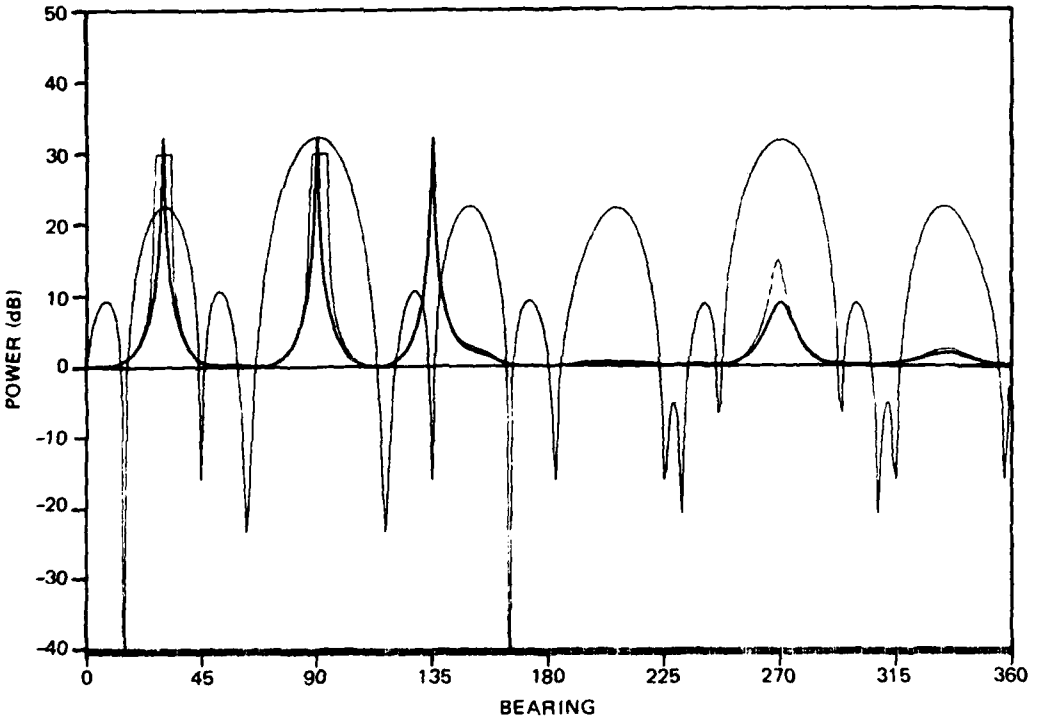

Figure 15. AAR and CBP. Mill's cross array; half-wavelength.

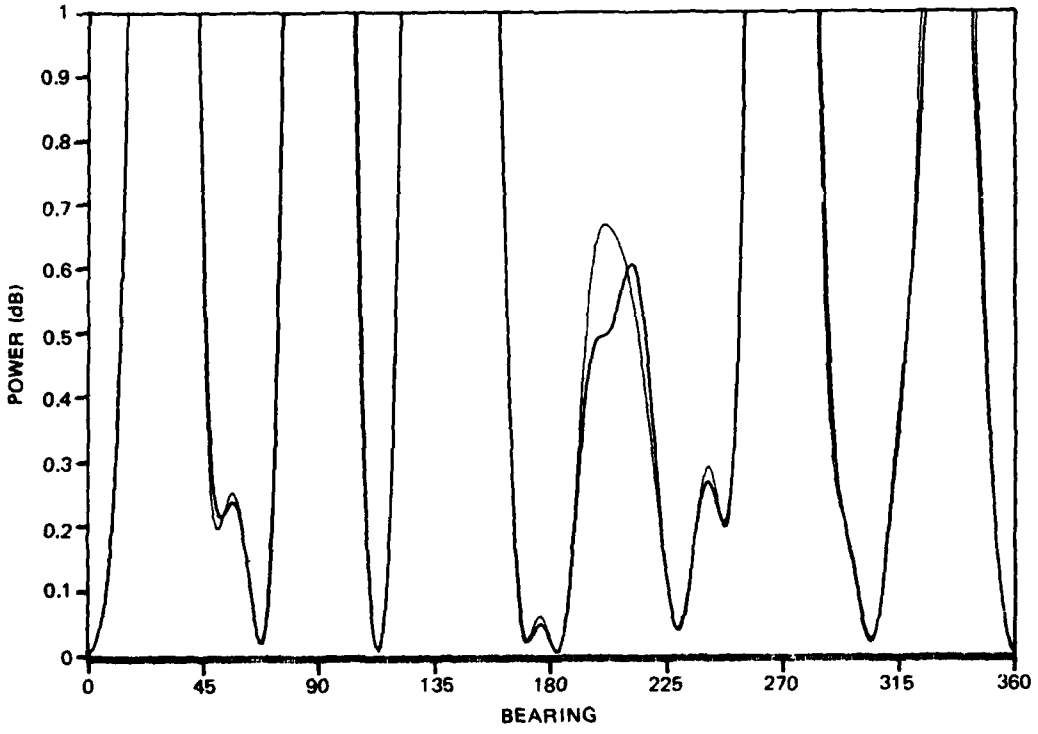

Figure 16. AAR detail. Mill's cross array; half-wavelength.

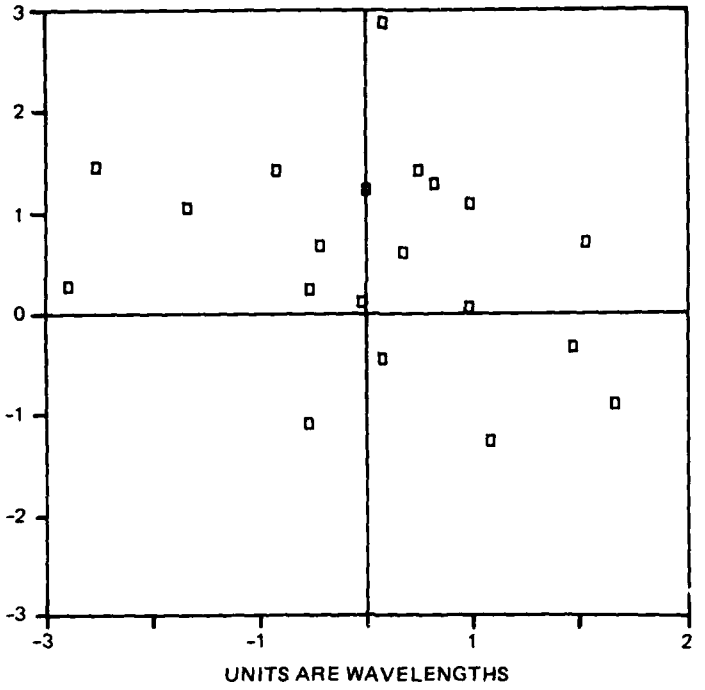

Figure 17. Random circular planar array; 20-element; diameter = 6 wavelengths.

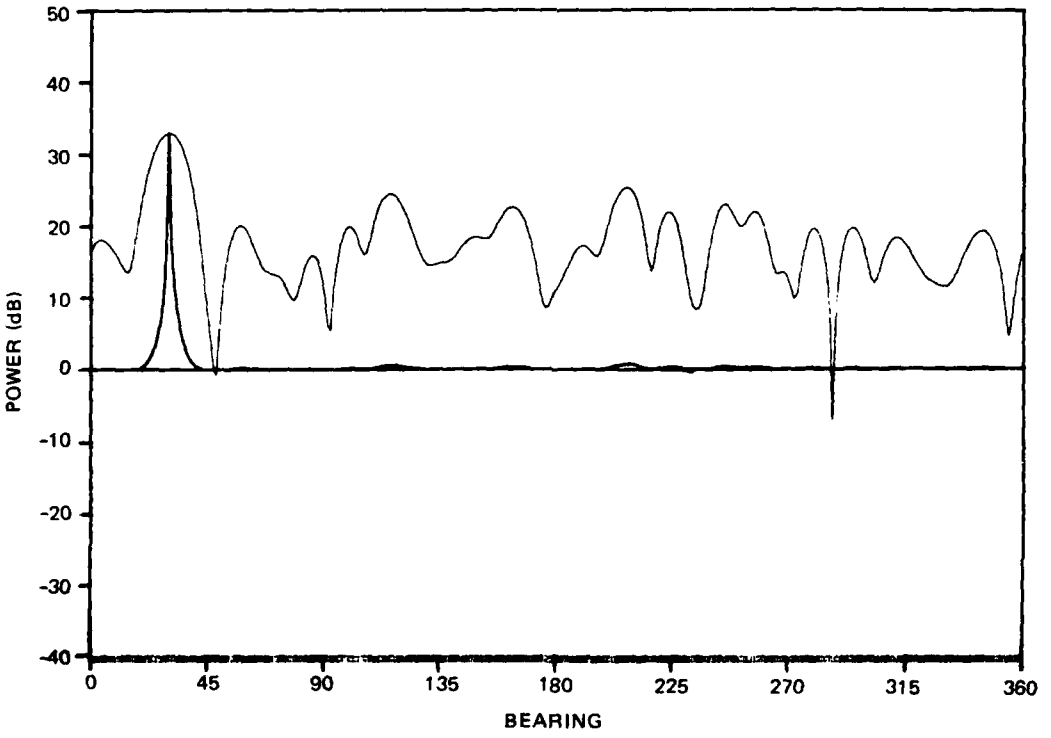

Figure 18. AAR and CBP. 20-element random circle; diameter = 6 wavelengths.

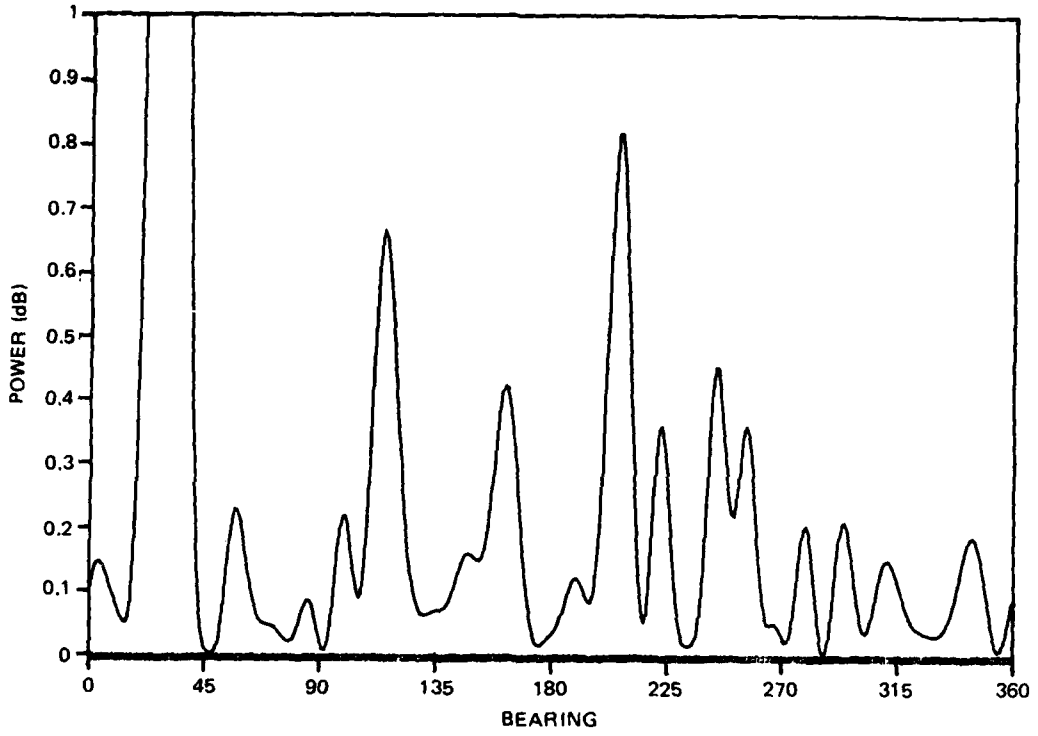

Figure 19. AAR detail. 20-element random circle; diameter = 6 wavelengths.

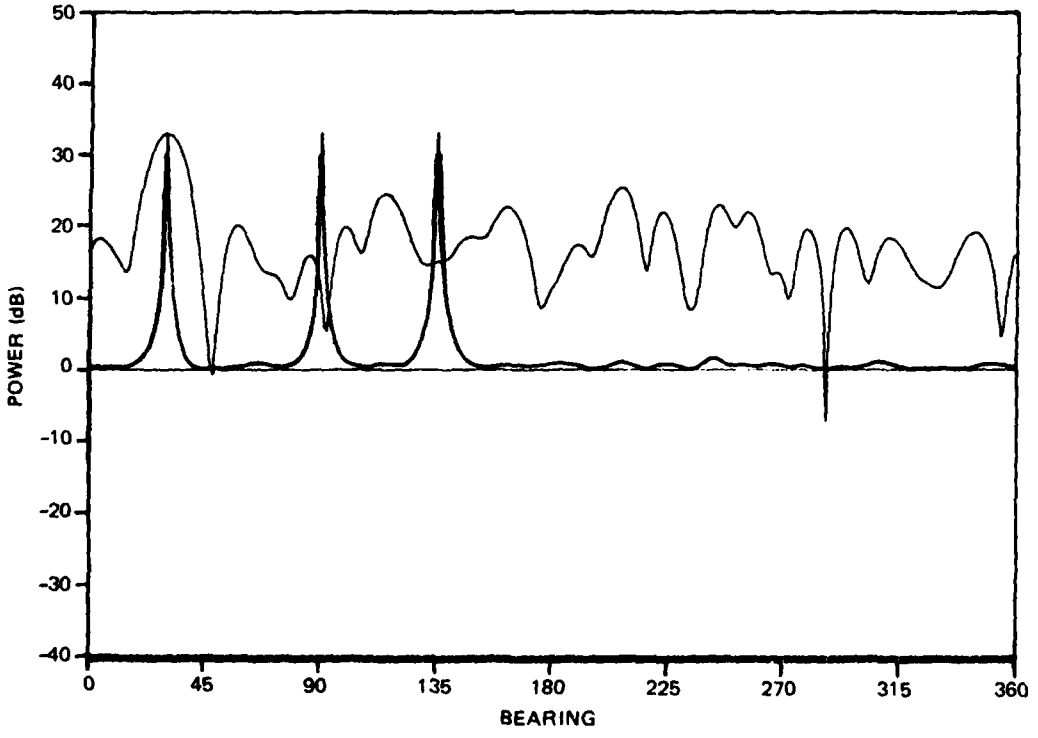

Figure 20. AAR and CBP. 20-element random circle; diameter = 6 wavelengths.

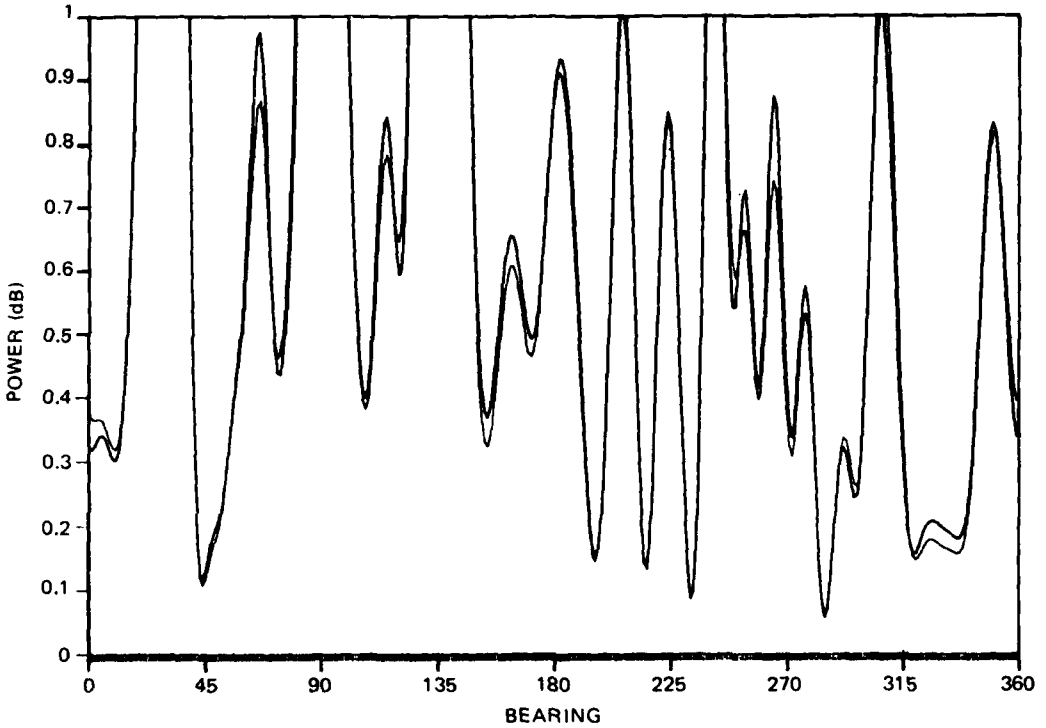

Figure 21. AAR detail. 20-element random circle; diameter = 6 wavelengths.

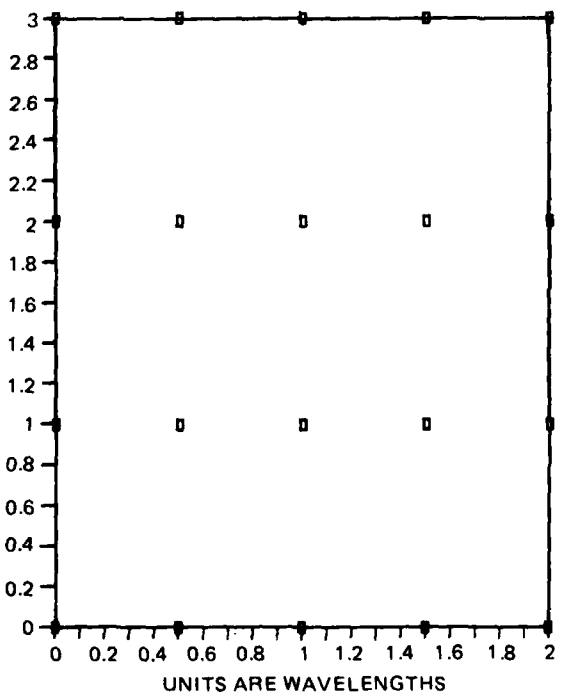

Figure 22. Deterministic positions. 20-element rectangular array.

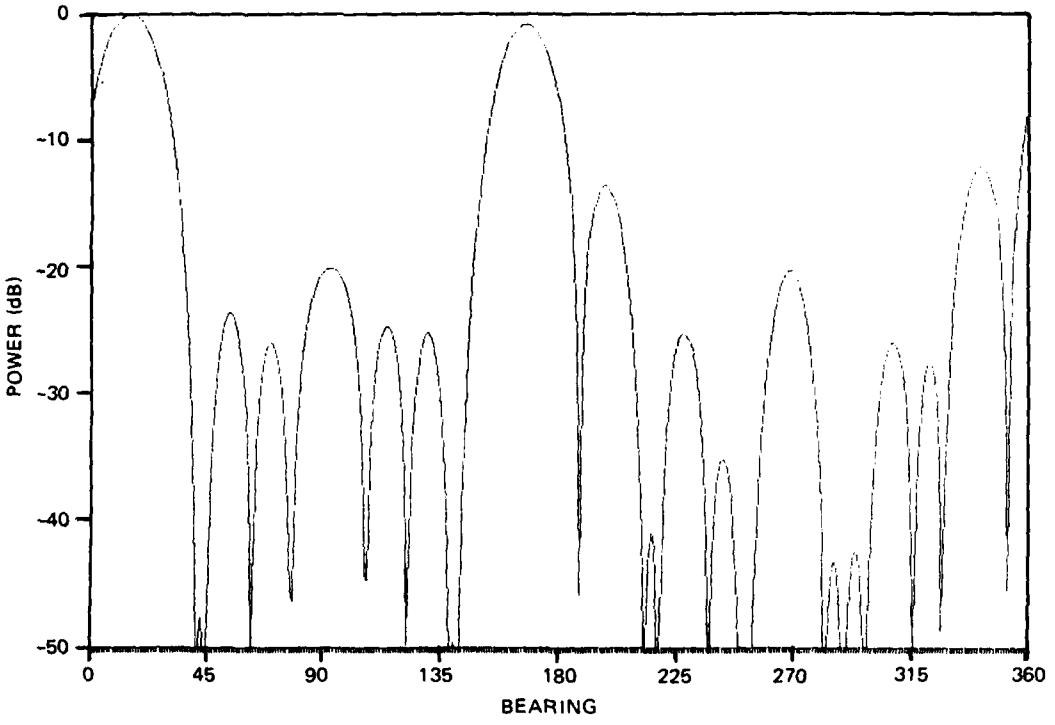

Figure 23. Conventional beampattern. 20-element rectangular array.

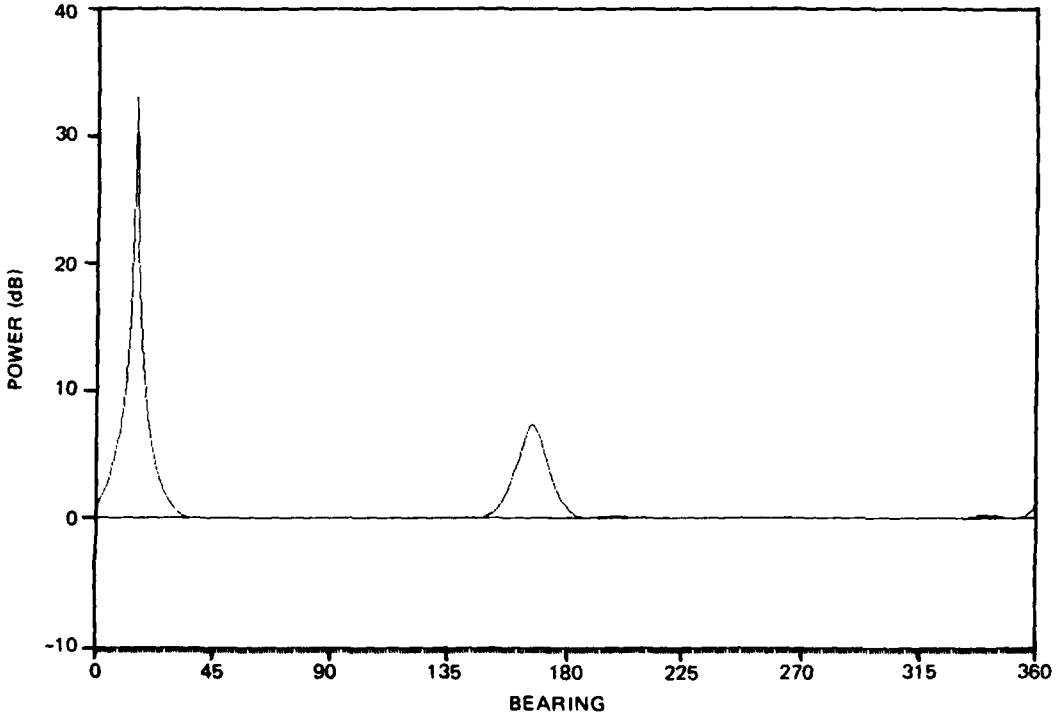

Figure 24. ME array response. Rectangular array; one signal.

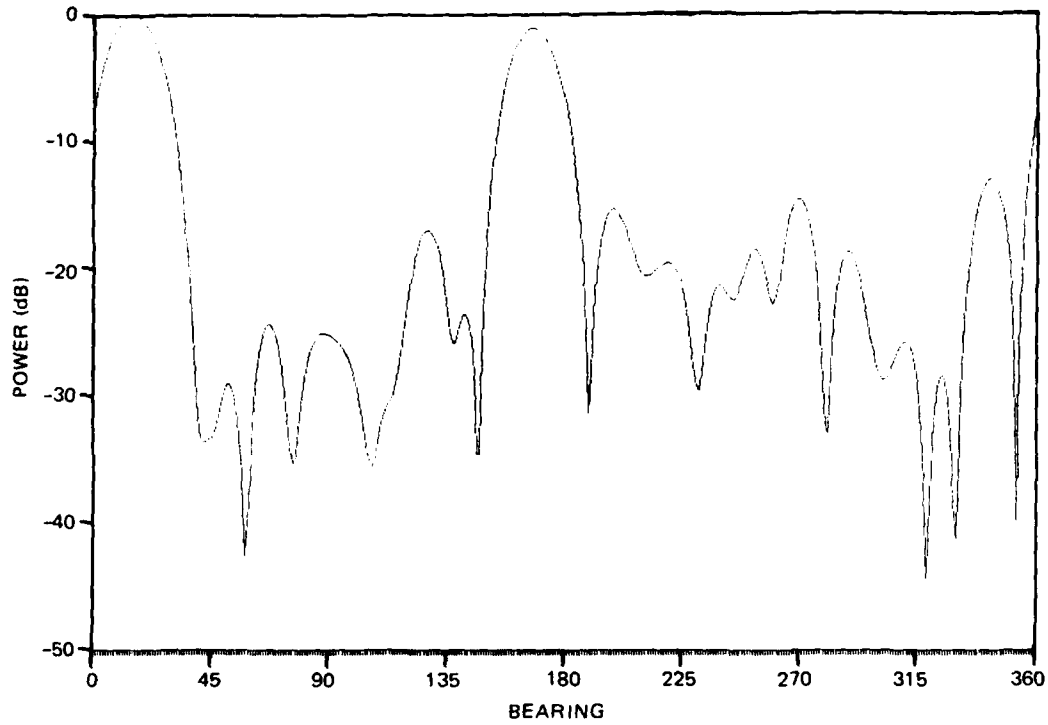

Figure 25. Conventional beampattern. Randomized rectangle epsilon = 0.1.

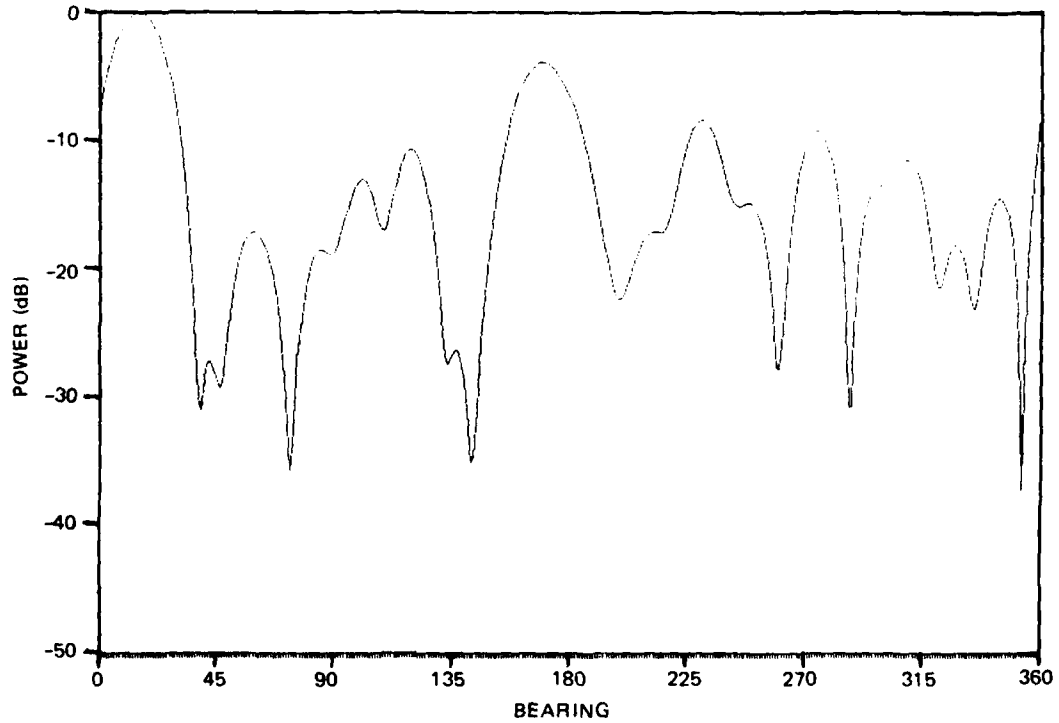

Figure 26. Conventional beampattern. Randomized rectangle epsilon = 0.3.

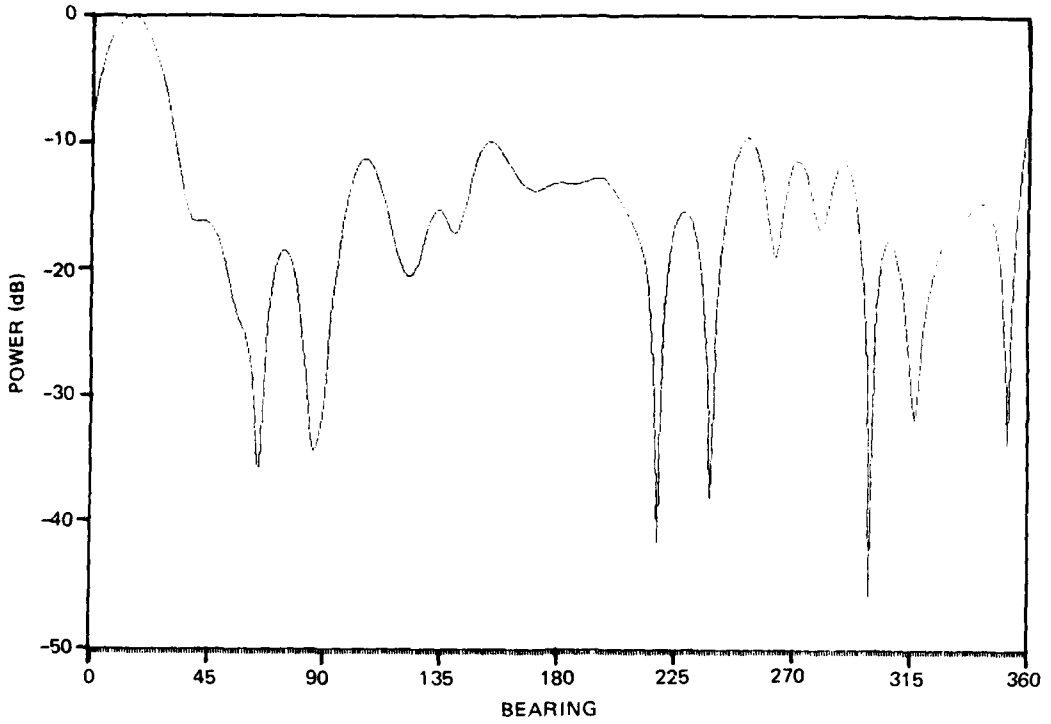

Figure 27. Conventional beampattern. Randomized rectangle epsilon = 0.5.

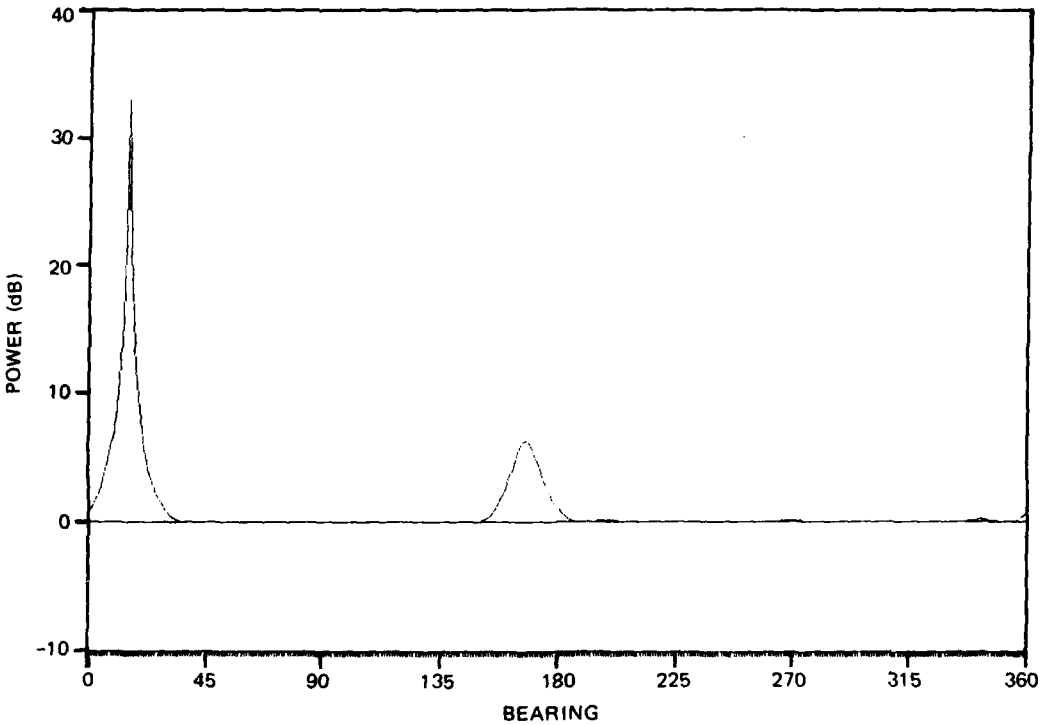

Figure 28. ME array response. Randomized rectangle epsilon = 0.1.

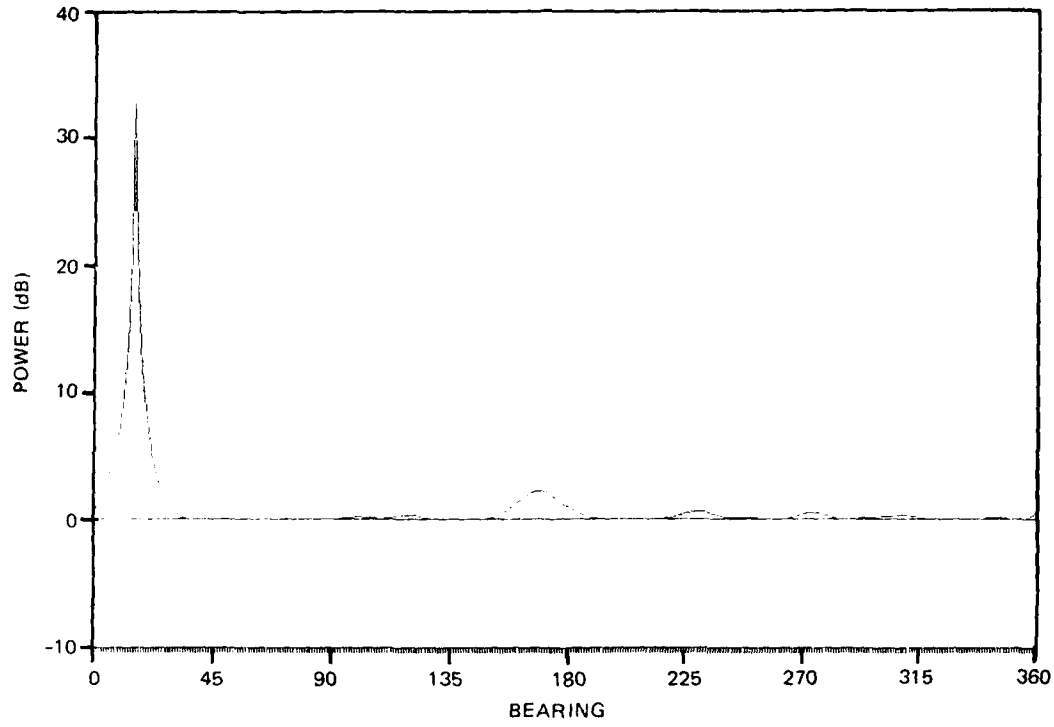

Figure 29. ME array response. Randomized rectangle epsilon = 0.3.

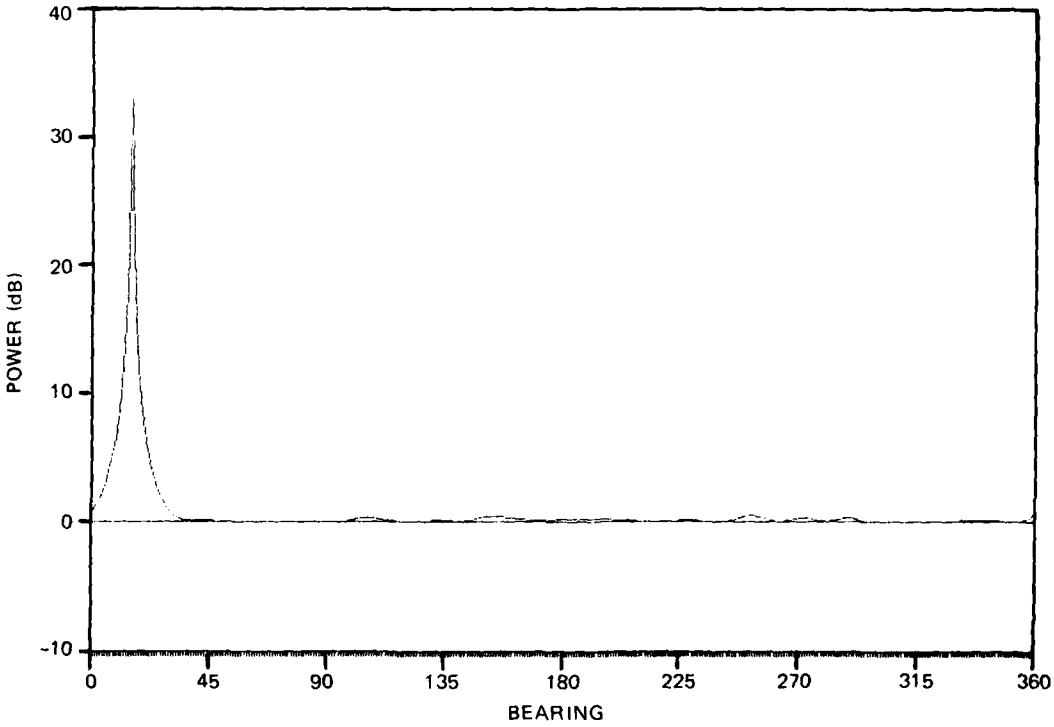

Figure 30. ME array response. Randomized rectangle epsilon = 0.5.

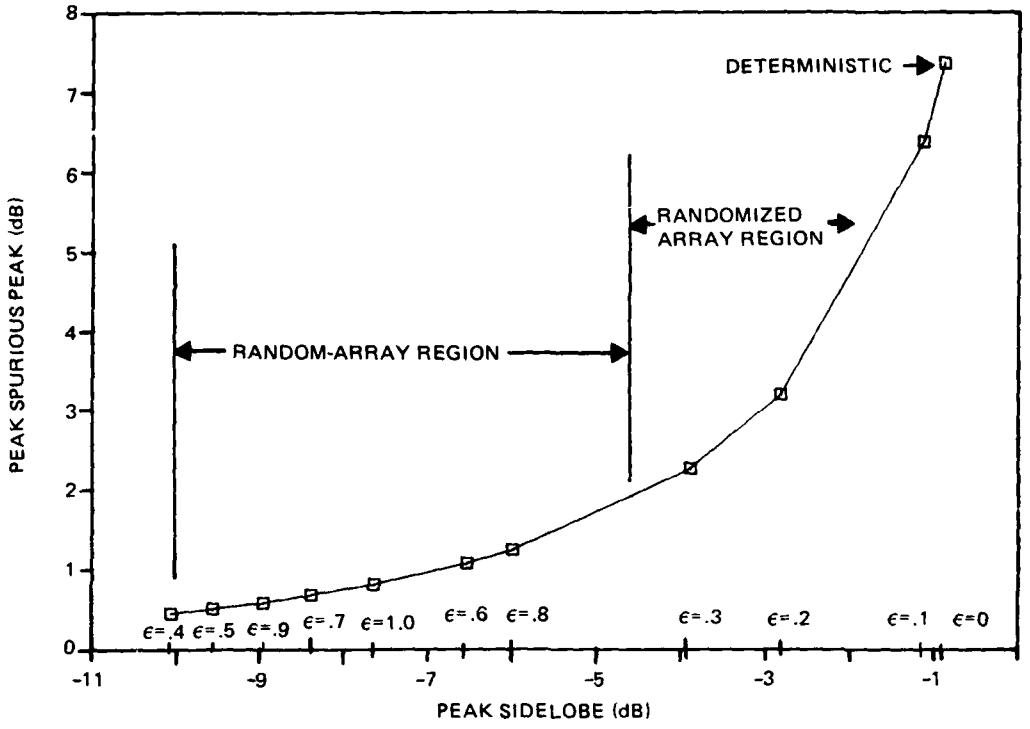

Figure 31. Peak sidelobe and spurious peak. 20-element randomized rectangle.

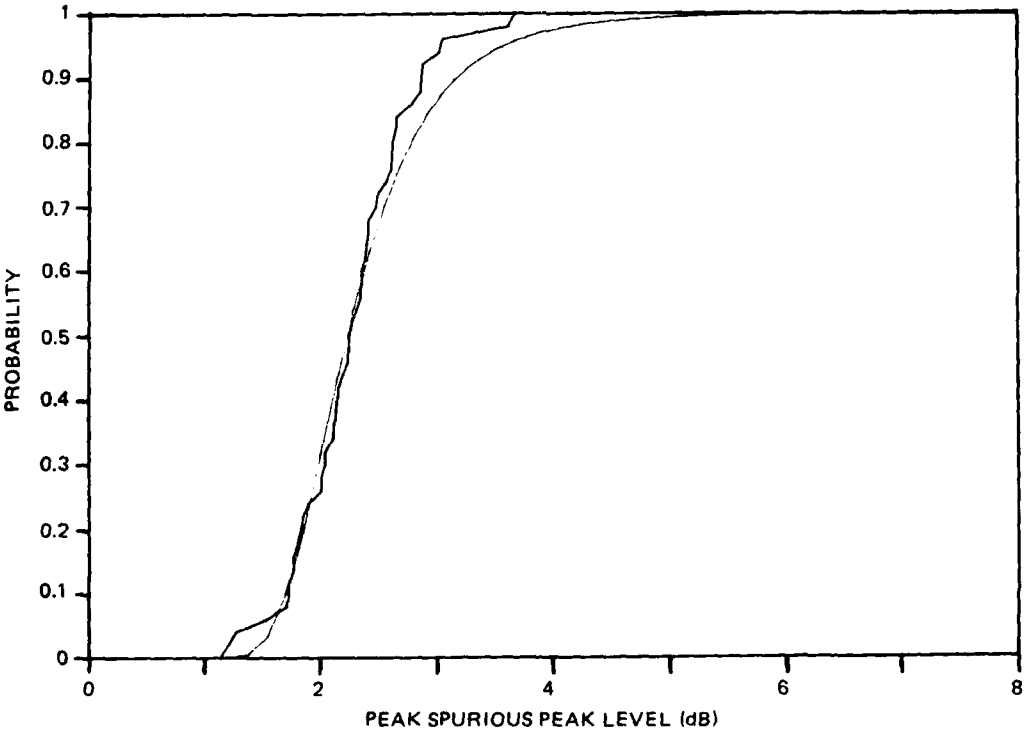

Figure 32. Peak spurious peak estimate. Random circle diameter = 10 wavelengths; N = 20 K = 3.

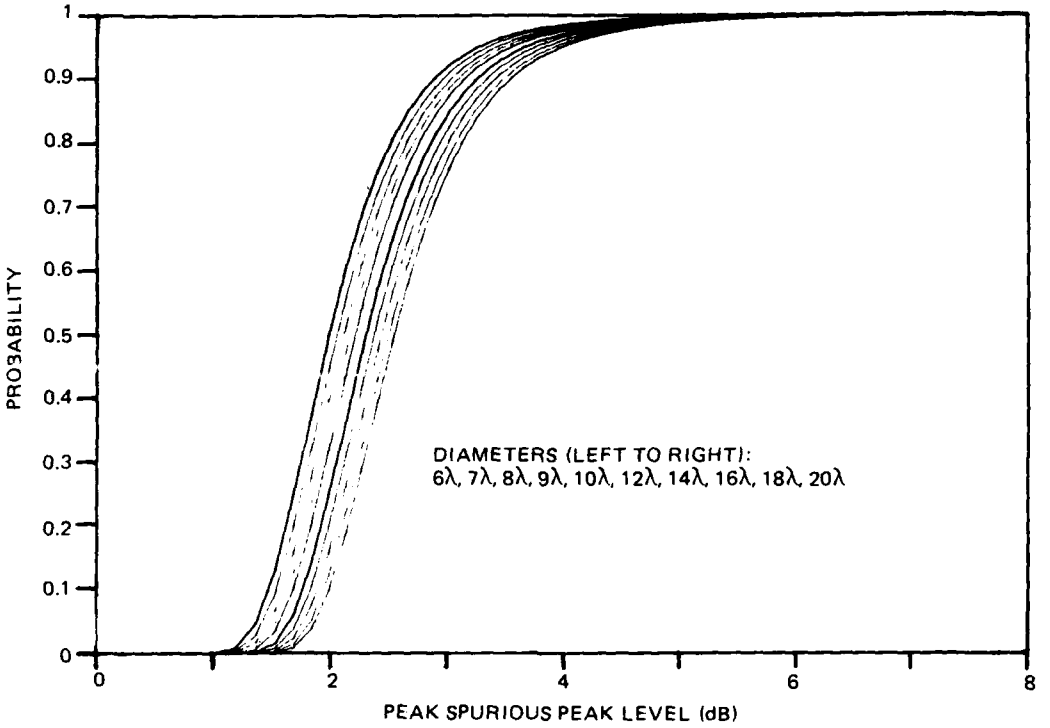

Figure 33. Adaptive array response. 20-elements; 3 signals.

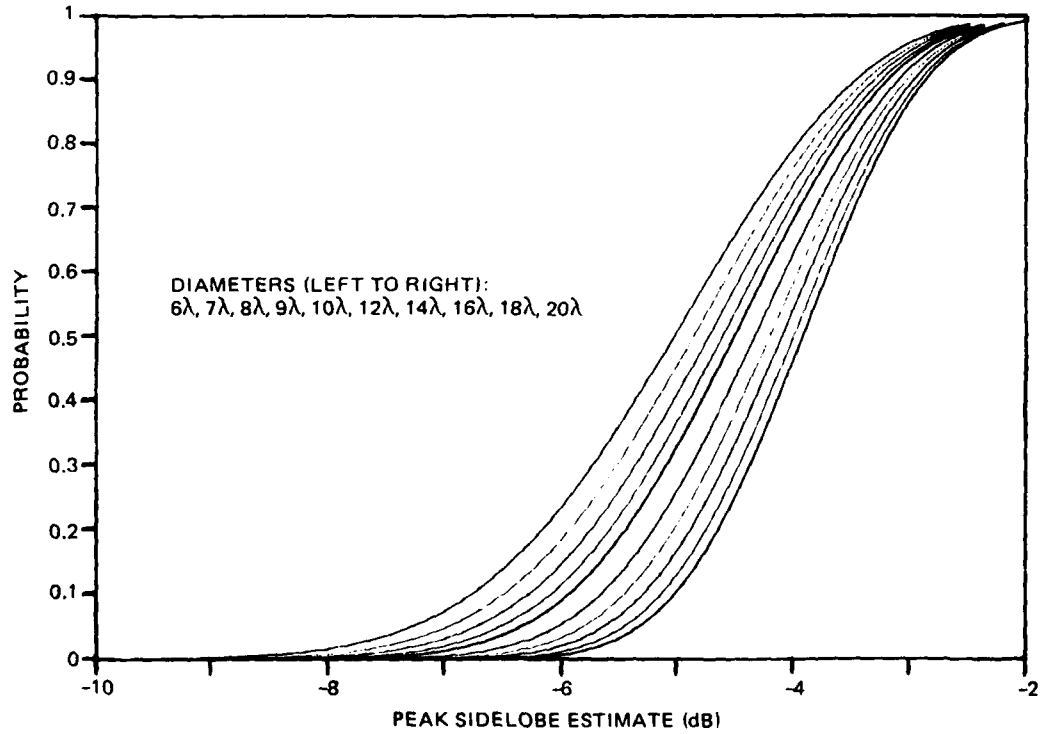

Figure 34. Random circular planar array. 20-elements; various diameters.

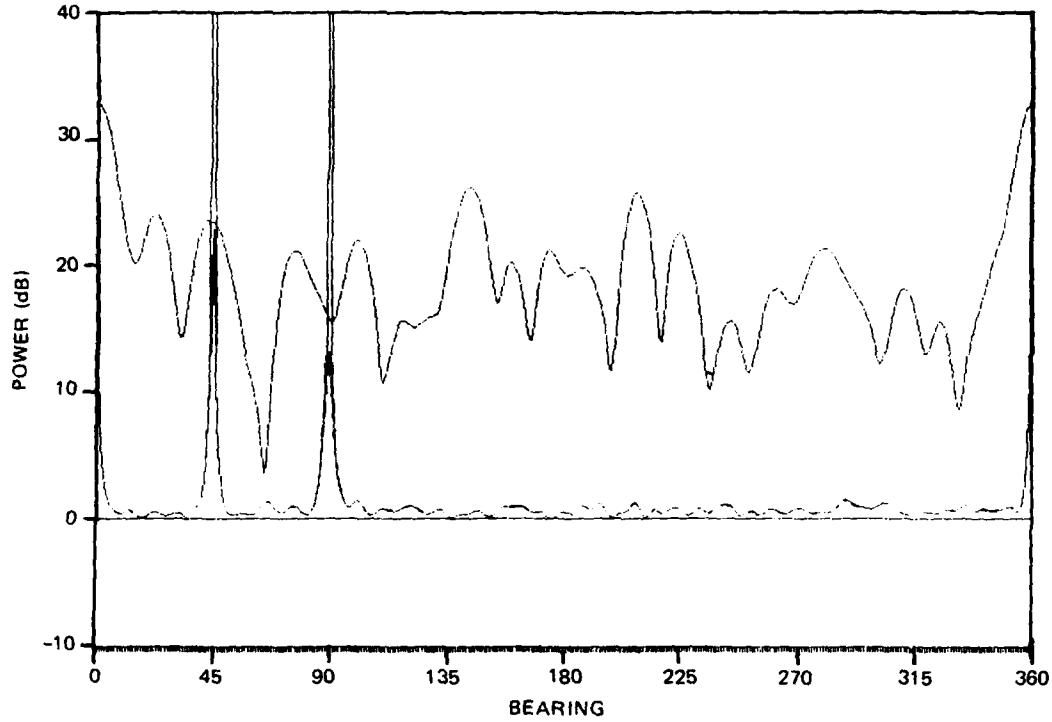

Figure 35. ME array response. Random circular array diameter = 6 wavelengths.

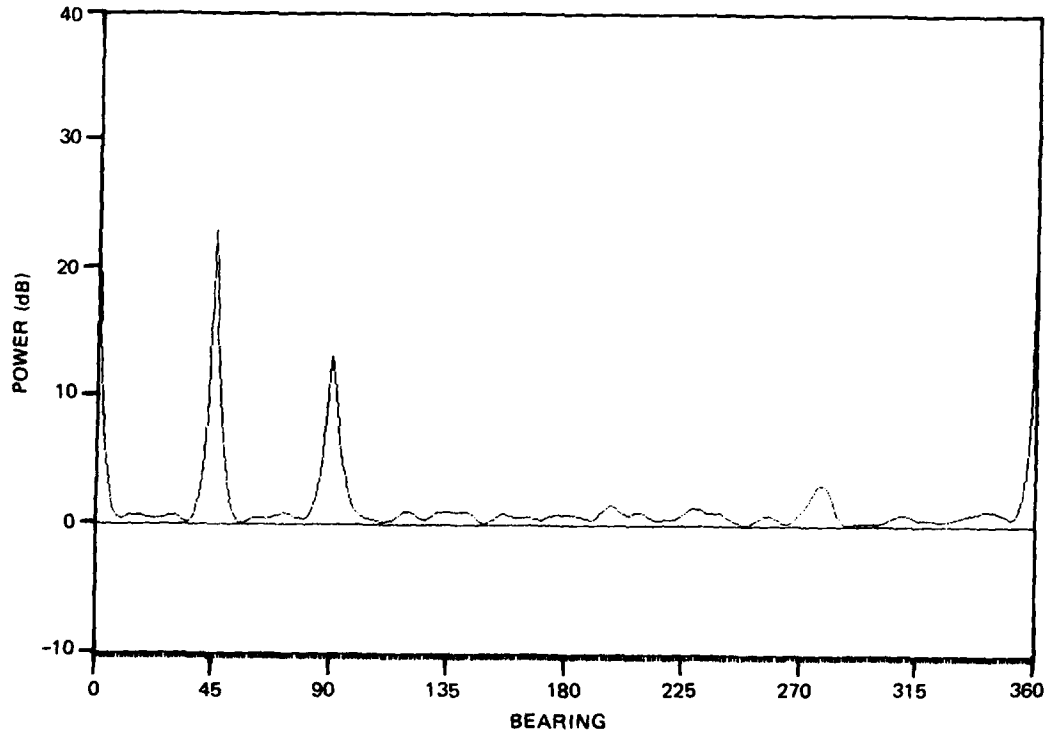

Figure 36. ME array response. Random circular array diameter = 8 wavelengths.

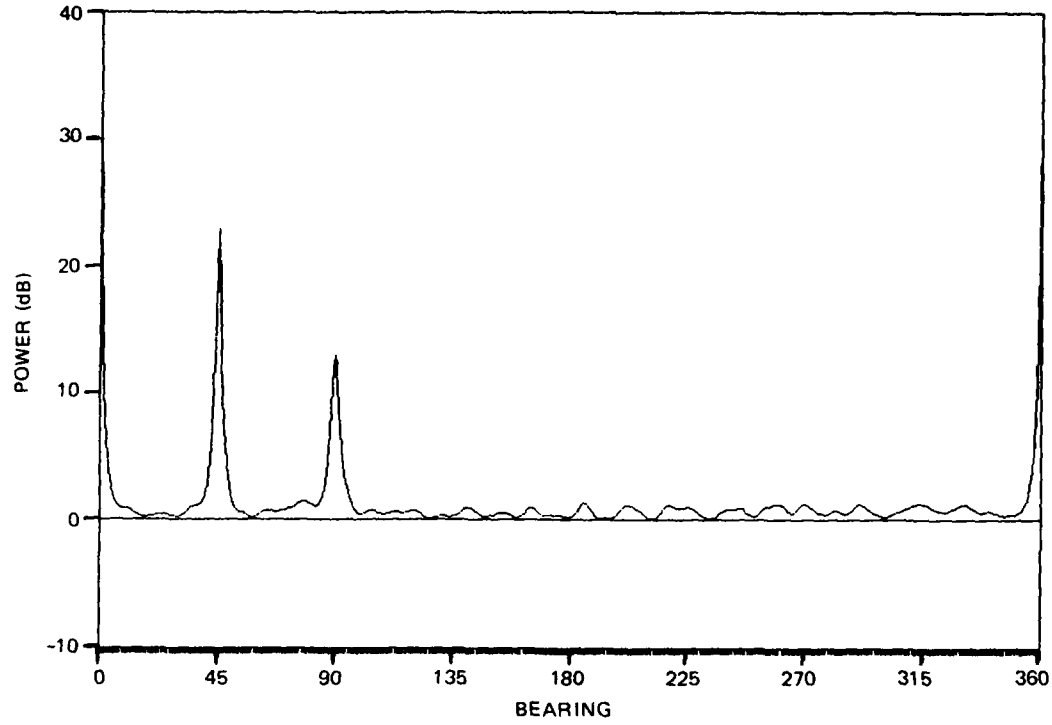

Figure 37. ME array response. Random circular array diameter = 10 wavelengths.

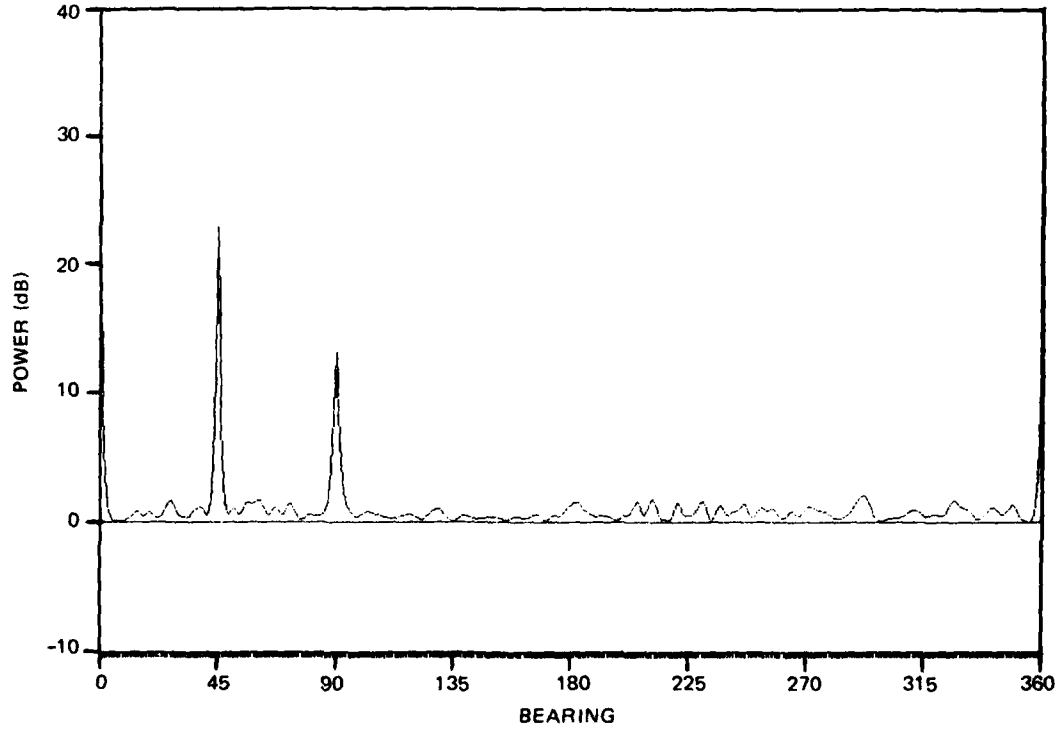

Figure 38. ME array response. Random circular array diameter = 14 wavelengths.

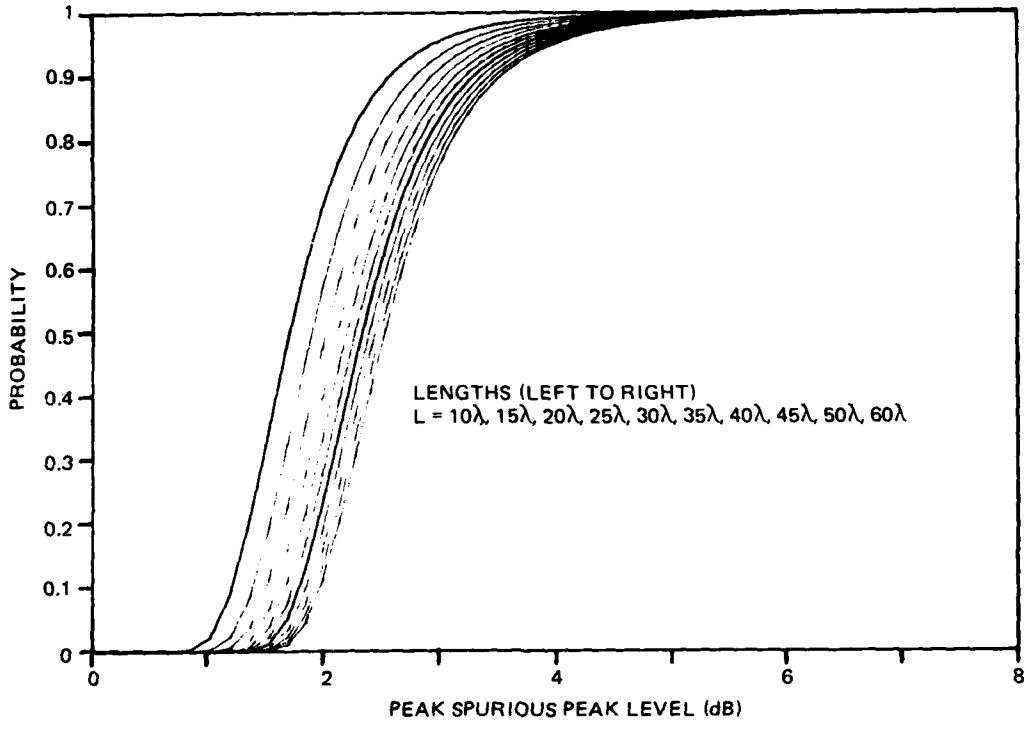

Figure 39. Adaptive spurious peak. 20-element line; 3 signals.

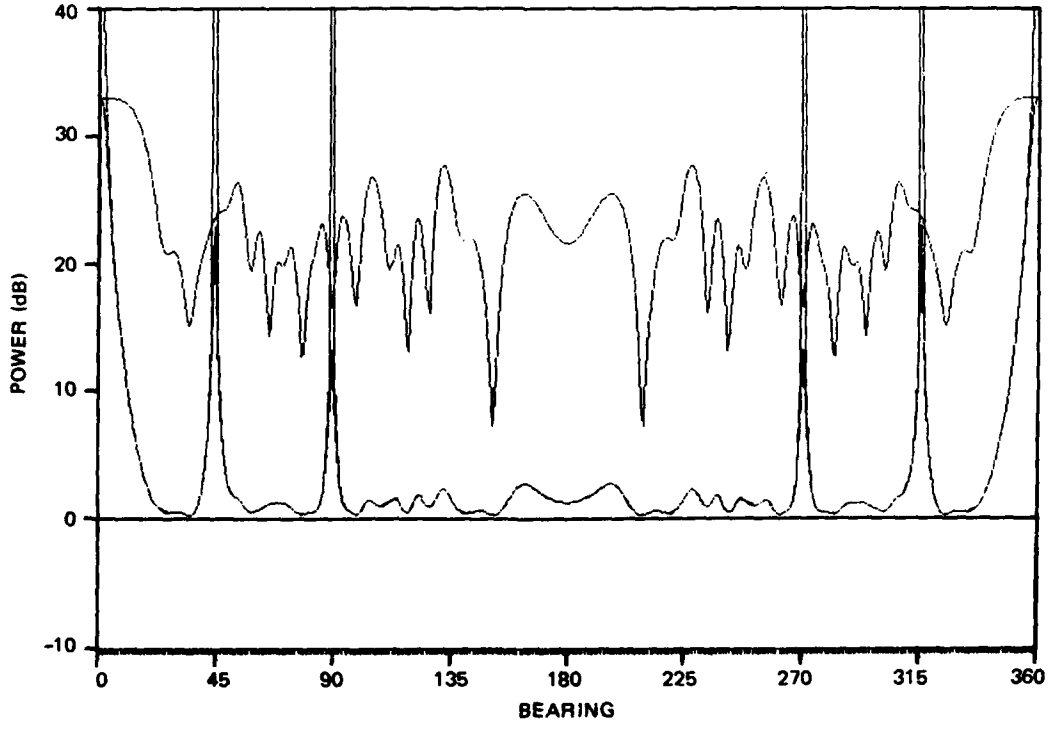

Figure 40. ME array response. 20-element random line; length = 10 wavelengths.

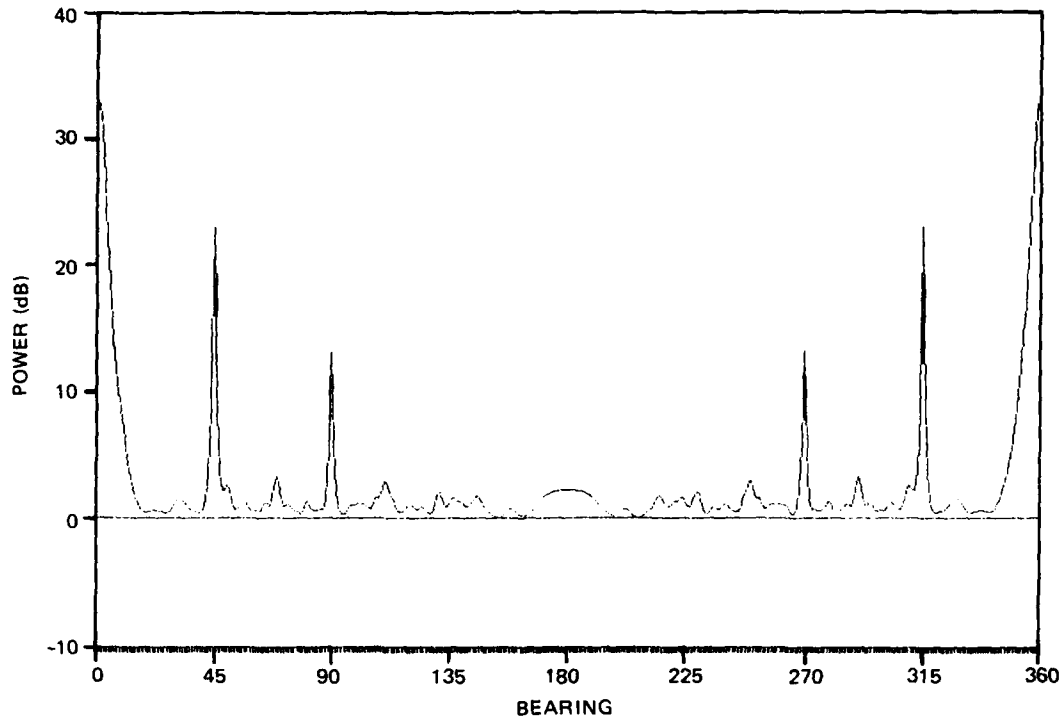

Figure 41. ME array response. 20-element random line; length = 20 wavelengths.

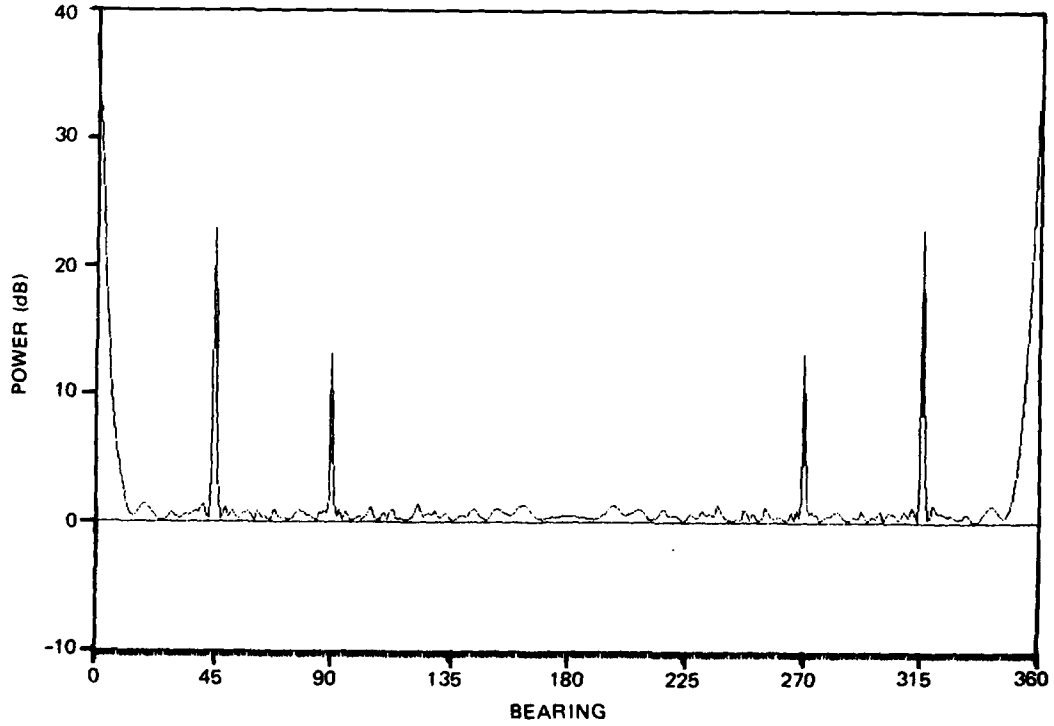

Figure 42. ME array response. 20-element random line; length = 30 wavelengths.

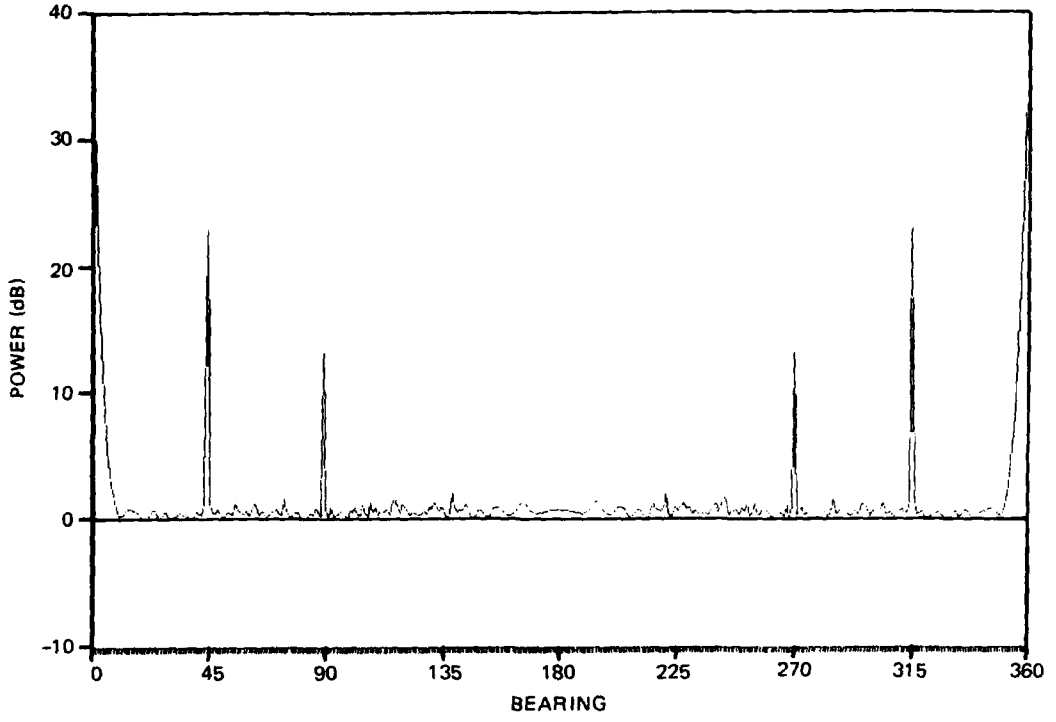

Figure 43. ME array response. 20-element random line; length = 50 wavelengths.

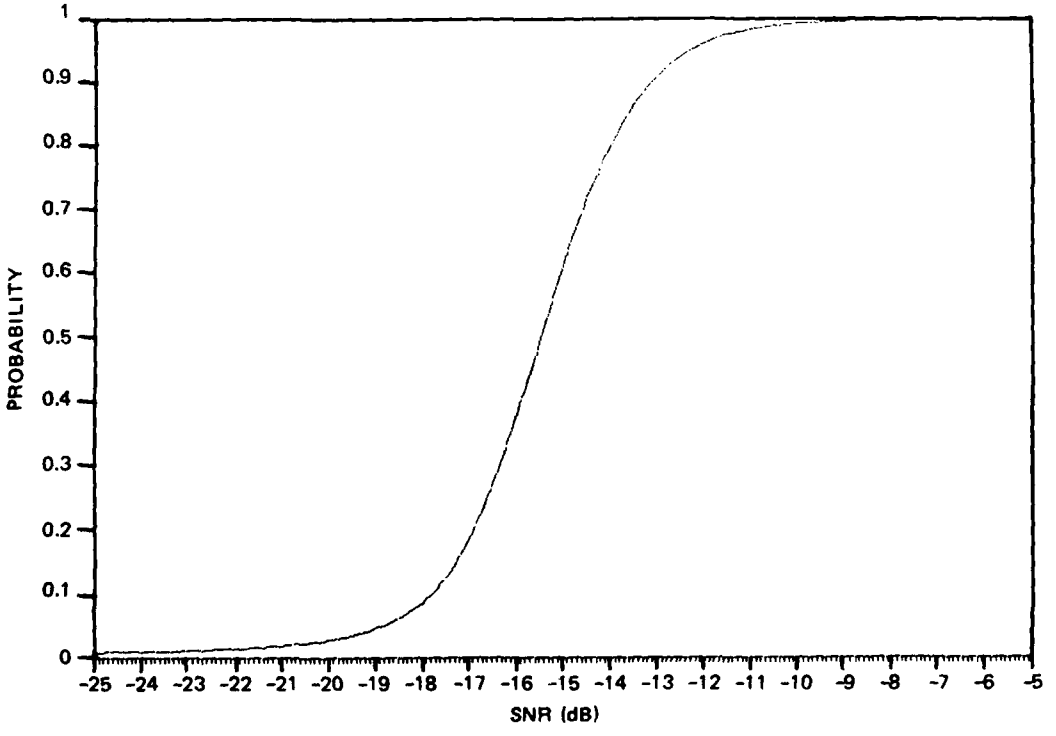

Figure 44. Detection probability. Random circular array; N = 20, n = 51, K = 2.

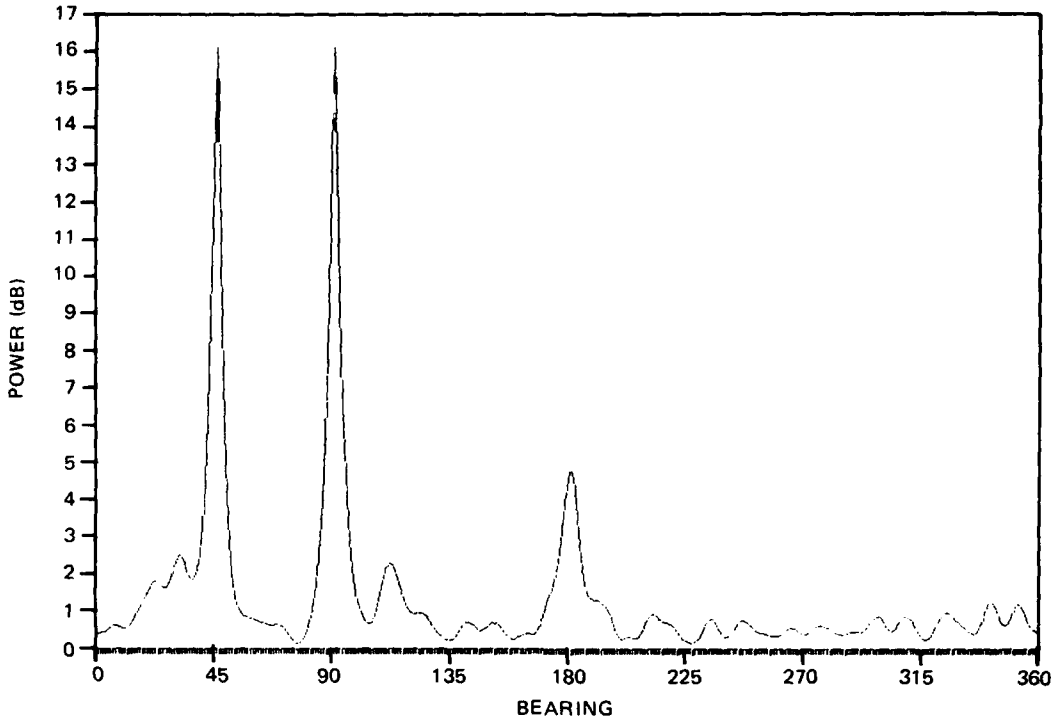

Figure 45. ME array response. Interest-signal SNR = -10.0 dB.

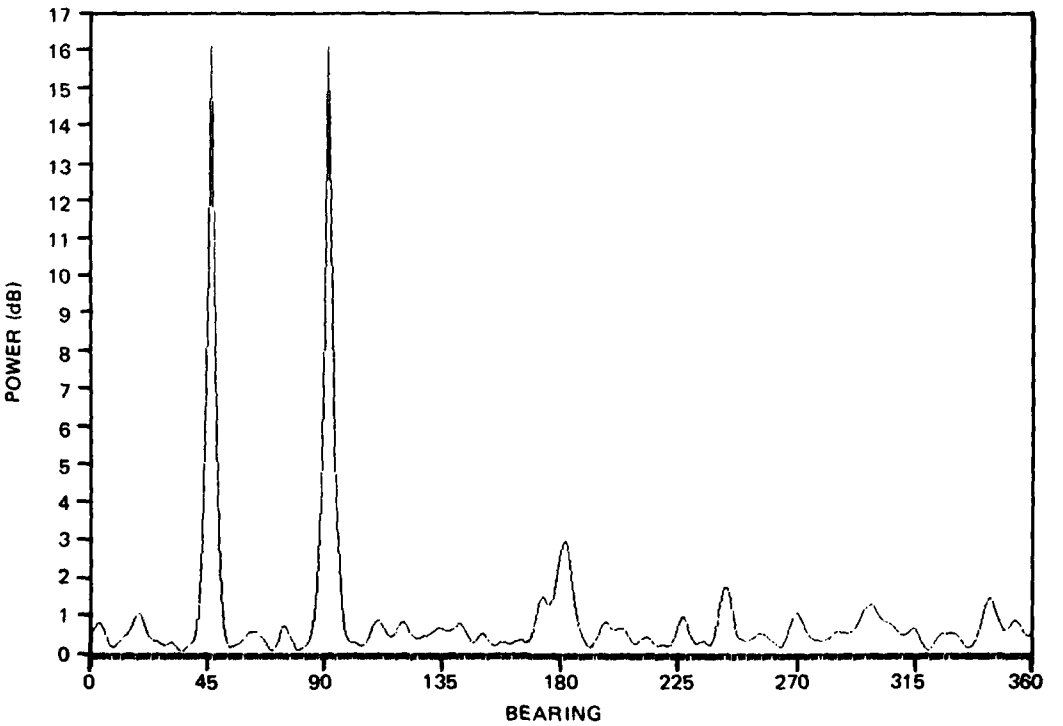

Figure 46. ME array response. Interest-signal SNR = -13.2 dB, case 1.

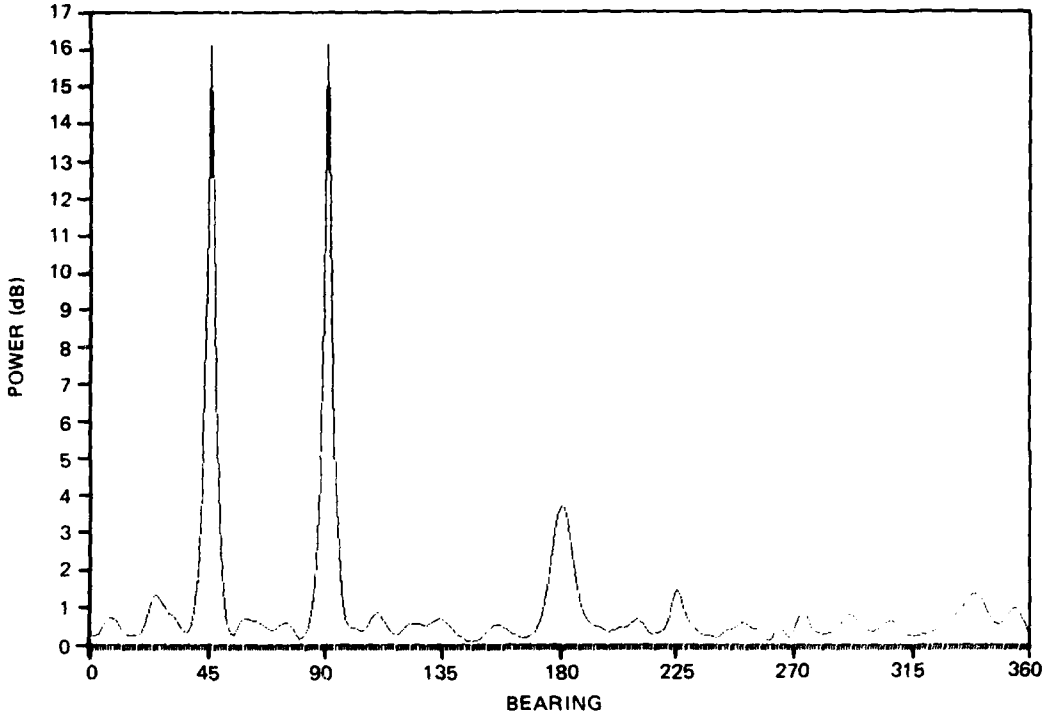

Figure 47. ME array response. Interest-signal SNR = -13.2 dB, case 2.

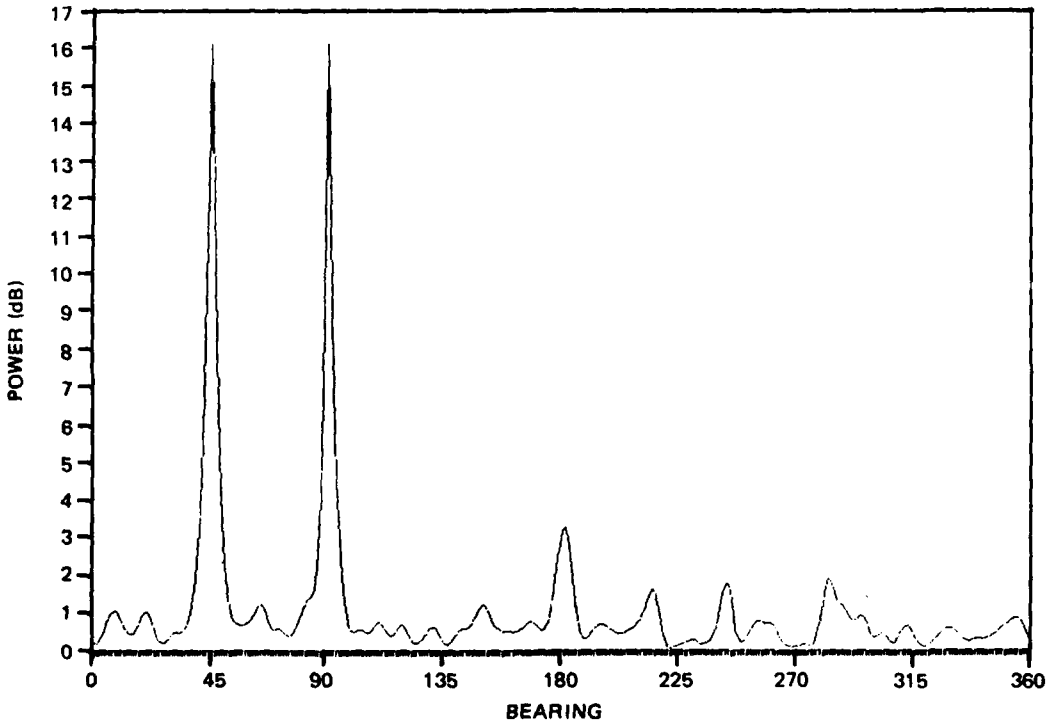

Figure 48. ME array response. Interest-signal SNR = -13.2 dB, case 3.

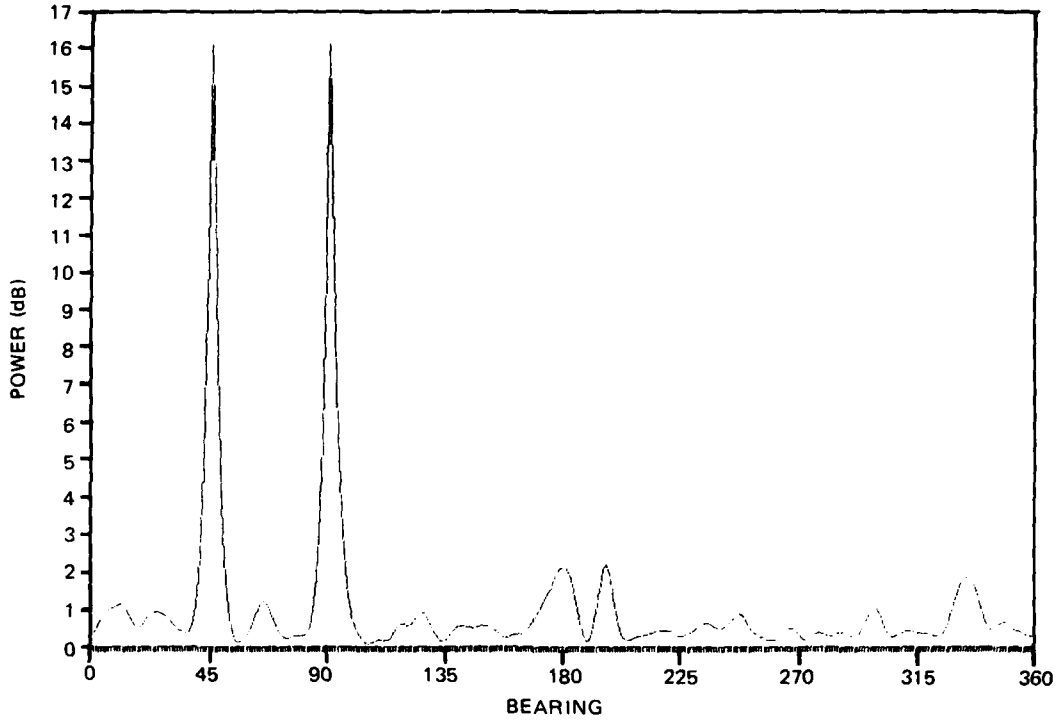

Figure 49. ME array response. Interest-signal SNR = -15.5 dB, case 1.

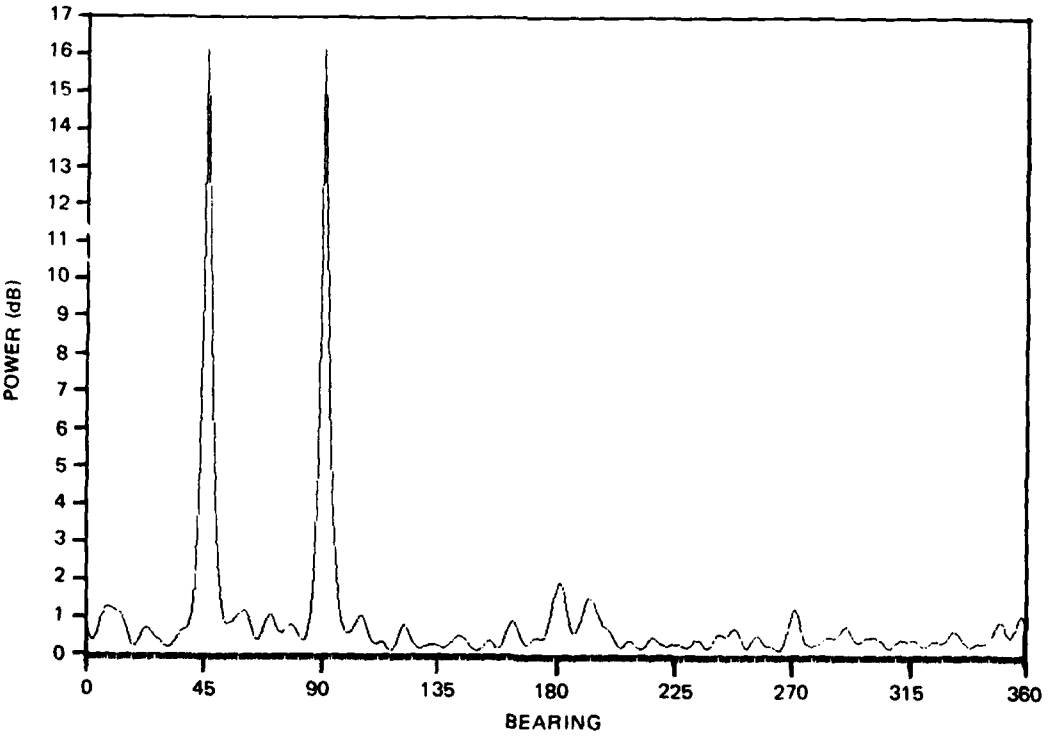

Figure 50. ME array response. Interest-signal SNR = -15.5 dB, case 2.

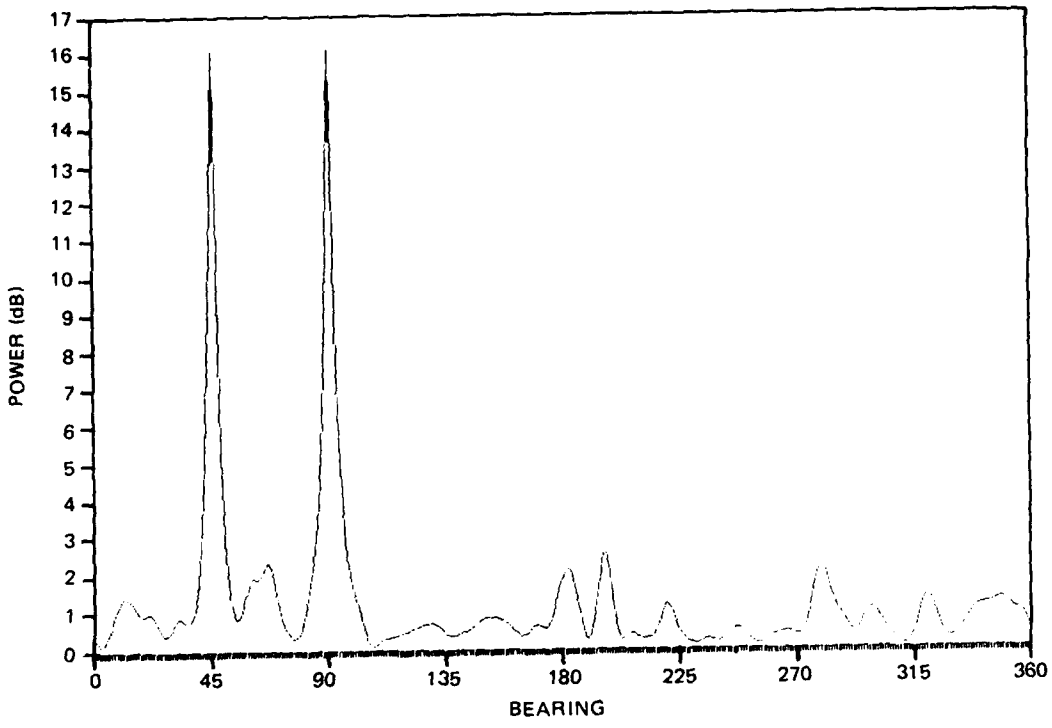

Figure 51. ME array response. Interest-signal SNR = -15.5 dB, case 3.

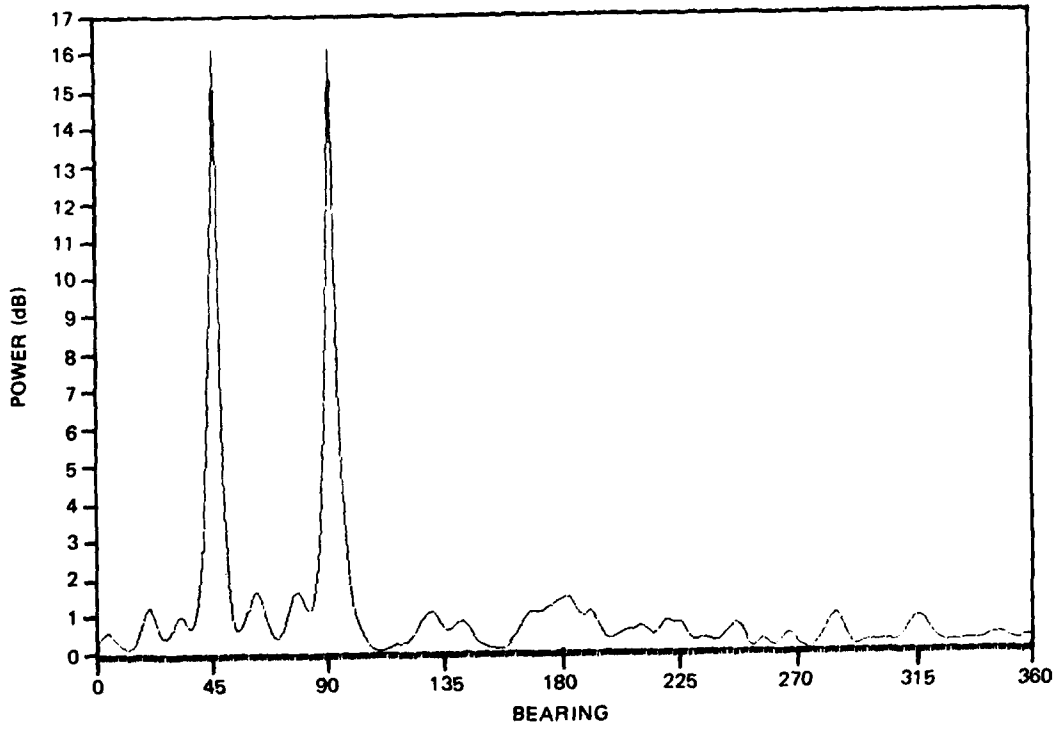

Figure 52. ME array response. Interest-signal SNR = -18.0 dB, case 1.

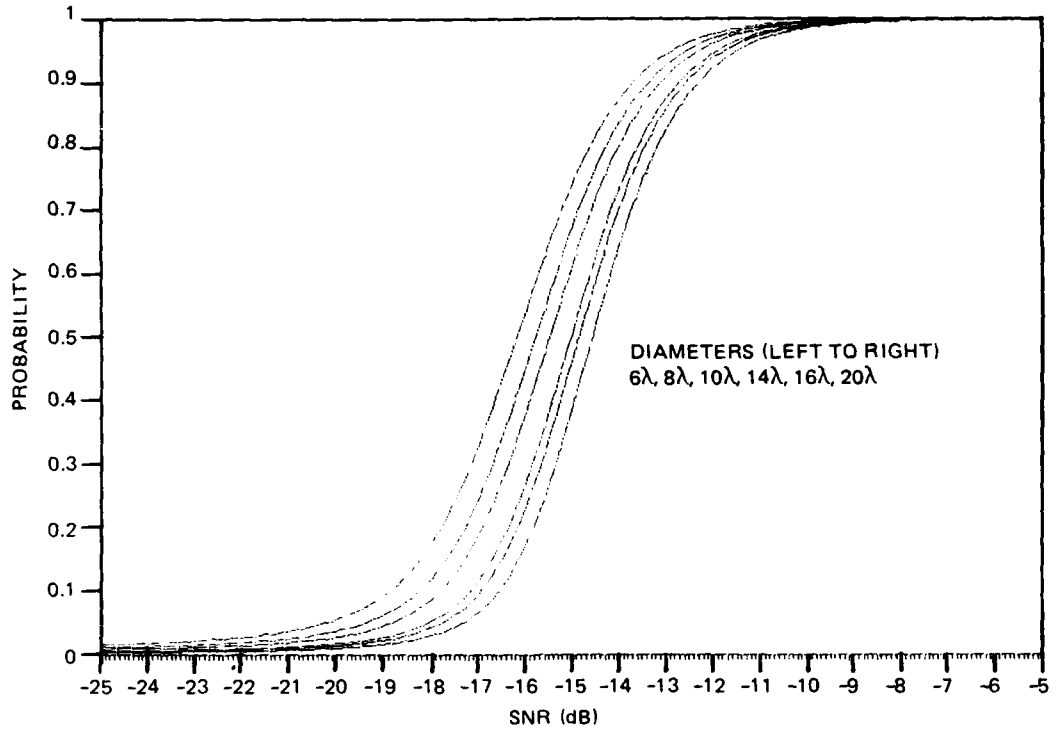

Figure 53. Detection probability. Random circular array; N = 20, K = 2.

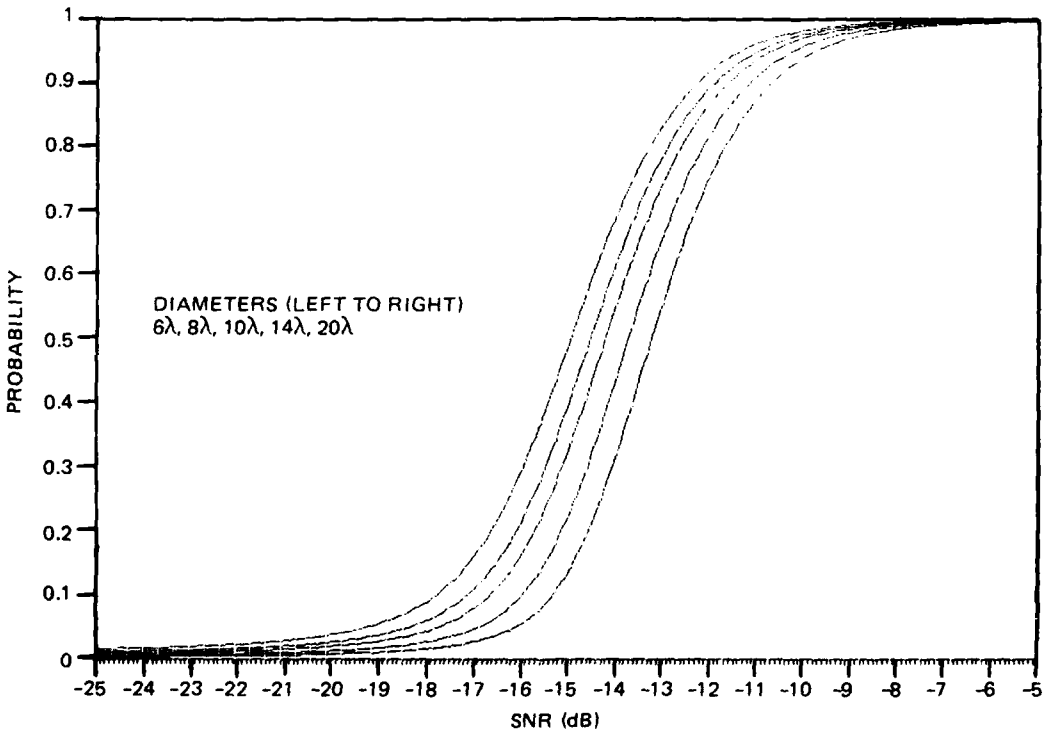

Figure 54. Detection probability. Random circular array; N = 20, K = 3.

IX. REFERENCES

Johnson, D.H. September 1982. "The Application of Spectral Estimation Methods to Bearing Estimation Problems," *Proceedings of the IEEE*, vol. 70, no. 4, pp. 1018–1028.

Johnson, D.H. and S. DeGraaf. August 1982. "Improving the Resolution of Bearing in Passive Sonar Arrays by Eigenvalue Analysis," *IEEE Transactions on Acoustics, Speech, and Signal Processing*, vol. ASSP-30, no. 4, pp. 638–647.

Schmidt, R.O. 1979. "Multiple Emitter Location and Parameter Estimation," Reprinted in *IEEE Transactions on Antennas and Propagation*, vol. AP-34, no. 3, March 1986.

Steinberg, B. 1976. *Principles of Aperture and Array System Design*, John Wiley and Sons, New York.

X. BIBLIOGRAPHY

Gabriel, W.F. March 1986. "Using Spectral Estimation Techniques in Adaptive Processing Antenna Systems," *IEEE Transactions on Antennas and Propagation*, vol. AP-34, no. 3.

Kay, S., and C. Demeure. December 1984. "The High-Resolution Spectrum Estimator — A Subjective Entity," *Proceedings of the IEEE*, vol. 72, no. 12, pp. 1815–1816.

Lockwood, J.C. April 1987. "Randomized Arrays," *Journal of the Acoustical Society of America*, vol. 81, no. 4, pp. 1009–1013.

APPENDIX I

Theorem

If $||\mathbf{P}|| < 1$, then $(\mathbf{I} - \mathbf{P})^{-1}$ exists and $||\mathbf{I} - (\mathbf{I} - \mathbf{P})^{-1}|| \leq \dfrac{||\mathbf{P}||}{1 - ||\mathbf{P}||}$.

Proof:

First, let $x \neq 0$. Then

$$||(\mathbf{I} - \mathbf{P})||x|| = ||x - \mathbf{P}x|| \geq ||x|| - ||\mathbf{P}x|| \geq ||x|| - ||\mathbf{P}|| \cdot ||x||$$

$$= (1 - ||\mathbf{P}||) \cdot ||x|| > 0$$

so that $(\mathbf{I} - \mathbf{P})x \neq 0$ and $\therefore (\mathbf{I} - \mathbf{P})^{-1}$ exists.

Next, we will show that $||(\mathbf{I} - \mathbf{P})^{-1}|| \leq \dfrac{1}{1 - ||\mathbf{P}||}$.

From $(\mathbf{I} - \mathbf{P})(\mathbf{I} - \mathbf{P})^{-1} = (\mathbf{I} - \mathbf{P})^{-1} - \mathbf{P}(\mathbf{I} - \mathbf{P})^{-1} = \mathbf{I}$,

we have that $(\mathbf{I} - \mathbf{P}^{-1} = \mathbf{I} + \mathbf{P}(\mathbf{I} - \mathbf{P})^{-1}$

$$\therefore ||(\mathbf{I} - \mathbf{P})^{-1}|| \leq ||\mathbf{I}|| + ||\mathbf{P}|| \cdot ||(\mathbf{I} - \mathbf{P})^{-1}|| = 1 + ||\mathbf{P}|| \cdot ||(\mathbf{I} - \mathbf{P})^{-1}||$$

$$(1 - ||\mathbf{P}||) \cdot ||(\mathbf{I} - \mathbf{P})^{-1}|| \leq 1$$

$$||(\mathbf{I} - \mathbf{P})^{-1}|| \leq \frac{1}{1 - ||\mathbf{P}||} .$$

Finally, from $(\mathbf{I} - \mathbf{P})(\mathbf{I} - \mathbf{P})^{-1} = (\mathbf{I} - \mathbf{P})^{-1} - \mathbf{P}(\mathbf{I} - \mathbf{P})^{-1} = \mathbf{I}$,

we have that $\mathbf{I} - (\mathbf{I} - \mathbf{P})^{-1} = -\mathbf{P}(\mathbf{I} - \mathbf{P})^{-1}$

$$\therefore ||\mathbf{I} - (\mathbf{I} - \mathbf{P})^{-1}|| \leq ||\mathbf{P}|| \cdot ||(\mathbf{I} - \mathbf{P})^{-1}|| \leq \frac{||\mathbf{P}||}{1 - ||\mathbf{P}||} .$$

APPENDIX II

Theorem

Let $X_1 X_2, \ldots, X_K$ be i.i.d. random variables with a probability density function

$$f(x_i) = \frac{1}{\sigma^2} e^{-x_i/\sigma^2} \; ; \quad x_i \geq 0 \; ; \quad i = 1,2, \ldots, K \; .$$

Then $Y = X_1 + X_2 + \ldots + X_K$ has a distribution with a p.d.f.

$$g(y) = \frac{1}{(K-1)!(\sigma^2)^K} y^{K-1} e^{-y/\sigma^2} \; ; \quad y \geq 0 \; .$$

Proof:

The Laplace transform of one of the X_i s is

$$L_r(f(x_i)) = \int_0^\infty e^{-rx_i} f(x_i) dx_i$$

$$= \int_0^\infty e^{-rx} \frac{1}{\sigma^2} e^{-x/\sigma^2} dx$$

$$= \frac{1}{\sigma^2} \int_0^\infty e^{-\left(r + \frac{1}{\sigma 2}\right)x} dx$$

$$= \frac{1}{\sigma^2} \cdot \frac{1}{-\left(r + \frac{1}{\sigma^2}\right)} e^{-\left(r + \frac{1}{\sigma 2}\right)x} \Bigg|_0^\infty$$

$$= \frac{1}{1 + \sigma^2 r} \; .$$

The Laplace transform of X is ∴

$$L_r(g(y)) = \prod_{L=1}^{K} L_r(f(x_i)) = \prod_{L=1}^{K} \frac{1}{1 + \sigma^2 r} = [1 + \sigma^2 r]^{-K} \qquad \text{(A-1)}$$

Here, $L_r(g(y))$ is analytic in the strip corresponding to $R_e[r] \geq -1/\sigma^2$. Rather than take the universe Laplace transform, we just take the Laplace transform of the p.d.f. in the proof statement. This is

$$L_r'(g(y)) = \int_0^\infty e^{-ry} \cdot \frac{1}{(K-1)!(\sigma^2)^K} y^{K-1} e^{-y/\sigma^2} dy$$

$$= \int_0^\infty \frac{y^{K-1}}{(K-1)!(\sigma^2)^K} e^{-\left(r + \frac{1}{\sigma^2}\right)x} dy .$$

Integrating by parts with $u = \dfrac{y^{K-1}}{-\left(r + \frac{1}{\sigma^2}\right)(K-1!)(\sigma^2)^K}$ yielding

$$du = \frac{y^{K-2}}{-\left(r + \frac{1}{\sigma^2}\right)(K-1!)(\sigma^2)^K} dy \text{ and } dv = -\left(r + \frac{1}{\sigma^2}\right) e^{-\left(r + \frac{1}{\sigma^2}\right) y} dy$$

so that $V = e^{-\left(r + \frac{1}{\sigma^2}\right) y}$ gives

$$L_r'(g(y)) = \int_0^\infty \frac{y^{K-2}}{-\left(r + \frac{1}{\sigma^2}\right)(K-2)!(\sigma^2)^K} e^{-\left(r + \frac{1}{\sigma^2}\right) y} dy .$$

Continuing in this fashion,

$$L_r'(g(y)) = \frac{1}{-\left(r + \frac{1}{\sigma^2}\right) K(\sigma^2)K} e^{-\left(r+\frac{1}{2}\right)y} \Bigg|_0^\infty \qquad \text{(A-2)}$$

$$= [1 + r\sigma^2]^{-K}$$

Noting the equality between (A-1) and (A-2) we now have the result.